

# Mechanisms of Intrinsic Beating Variability in Cardiac Cell Cultures and Model Pacemaker Networks

Julien G. C. Ponard, Aleksandar A. Kondratyev, and Jan P. Kucera

Department of Physiology, University of Bern, Bülhlplatz 5 CH-3012 Bern, Switzerland

**ABSTRACT** Heart rate variability (HRV) exhibits fluctuations characterized by a power law behavior of its power spectrum. The interpretation of this nonlinear HRV behavior, resulting from interactions between extracardiac regulatory mechanisms, could be clinically useful. However, the involvement of intrinsic variations of pacemaker rate in HRV has scarcely been investigated. We examined beating variability in spontaneously active incubating cultures of neonatal rat ventricular myocytes using microelectrode arrays. In networks of mathematical model pacemaker cells, we evaluated the variability induced by the stochastic gating of transmembrane currents and of calcium release channels and by the dynamic turnover of ion channels. In the cultures, spontaneous activity originated from a mobile focus. Both the beat-to-beat movement of the focus and beat rate variability exhibited a power law behavior. In the model networks, stochastic fluctuations in transmembrane currents and stochastic gating of calcium release channels did not reproduce the spatiotemporal patterns observed *in vitro*. In contrast, long-term correlations produced by the turnover of ion channels induced variability patterns with a power law behavior similar to those observed experimentally. Therefore, phenomena leading to long-term correlated variations in pacemaker cellular function may, in conjunction with extracardiac regulatory mechanisms, contribute to the nonlinear characteristics of HRV.

## INTRODUCTION

The normal heartbeat is initiated in the sinoatrial node (SAN), a pacemaking structure that generates action potentials which propagate across the atria and ventricles and trigger their rhythmic contractions. Although the heartbeat is a periodical phenomenon, heart rate varies continuously with time. These variations adjust the cardiac output to the demand of the organism and are essentially controlled by regulatory reflexes mediated by the autonomic nervous system (1–3).

During the past decades, numerous efforts have been invested to extract clinically relevant information from the analysis of the variations of heart rate on a beat-to-beat basis (4,5). A widespread method for the analysis of heart rate variability (HRV) is to decompose the variations of heart rate into a spectrum of distinct frequency components by means of Fourier analysis or autoregressive modeling (6–8). When applied to human subjects, this analysis reveals two frequency ranges in which periodic variations in heart rate prevalently occur: a high frequency range (centered around 0.25 Hz) and a low frequency range (centered around 0.1 Hz). It is well established that these periodic variations are related to breathing and the regulation of arterial blood pressure, respectively, and that they are mediated by the autonomic nervous system (9,10). The quantitative analysis of the high frequency and the low frequency components is thus widely applied to evaluate the balance between the sympathetic and the parasympathetic branches of the autonomic nervous system in a variety of clinical settings (4,11).

However, the major component of HRV occurs at frequencies below the low frequency range ( $<0.04$  Hz). It is known that in the range  $10^{-4}$ – $10^{-2}$  Hz, the power spectrum of HRV does not exhibit periodic components but exhibits a so-called power law behavior (12–15). The term “power law” describes the relationship between two quantities  $x$  and  $y$  if this relationship can be expressed as  $y = A \times x^k$  or  $y \sim x^k$ , where  $k$  is called the “power law exponent”. Power laws are among the most frequent laws that describe fractal objects, i.e., objects that have a fine structure at each scale and appear similar at all scales of magnification (16). In a time series (e.g., of heart rate or interbeat intervals), this property of self-similarity reflects the presence of long-term correlations across a wide range of temporal scales (17,18). In the context of HRV, the notion of power law behavior refers to the power law relating the power spectral density (PSD) of HRV and frequency ( $f$ ), expressed as  $\text{PSD}(f) \sim f^\beta$ , where  $\beta$  is the power law exponent. The power law, reflecting the fractal properties of HRV, can be graphically visualized in a double logarithmic plot of  $\text{PSD}(f)$  versus  $f$ , in which the spectrum follows a line with a slope corresponding to  $\beta$ . In healthy subjects, the exponent  $\beta$  is close to  $-1$ .

In clinical studies of HRV, it has been shown empirically that certain disease states are associated with significant modifications of the power law exponent  $\beta$ . In particular, a more negative  $\beta$  (a steeper slope of the power spectrum) has been found in myocardial infarction patients and in patients after cardiac transplantation (19). It has also been shown that a more negative  $\beta$  occurs in patients prone to ventricular fibrillation (20) and discriminates patients with increased mortality (21). Thus,  $\beta$  represents a predictive risk-stratification marker, as more negative values of  $\beta$  are associated with an increased probability of sudden cardiac death (19,20,22–24). In other

Submitted June 21, 2006, and accepted for publication January 30, 2007.

Address reprint requests to Jan P. Kucera, MD, Dept. of Physiology, University of Bern, Bülhlplatz 5 CH-3012 Bern, Switzerland. Tel.: 41-31-631-87-59; Fax: 41-31-631-46-11; E-mail: kucera@pyl.unibe.ch.

© 2007 by the Biophysical Society

0006-3495/07/05/3734/19 \$2.00

doi: 10.1529/biophysj.106.091892

studies, HRV was evaluated using detrended fluctuation analysis, a fractal analytical method to quantify long-term correlations analogous to the determination of the slope  $\beta$  (25). These studies demonstrated alterations of detrended fluctuation parameters in, e.g., sleep apnea patients (26) and in asymptomatic relatives of patients with familial dilated cardiomyopathy (27).

These findings indicate that the analysis of HRV using fractal methods represents a clinically relevant evaluation tool. However, to date, the physiological mechanisms underlying the power-law behavior of HRV have scarcely been studied. To obtain the full benefit from these analyses, it is, therefore, essential to gain understanding of the underlying physiology to improve the specificity of risk stratification during clinical evaluation and the development of directed patient follow-up protocols and specific therapies.

It is an accepted notion that the aperiodic variations characteristic of HRV at low frequencies are the result of complex nonlinear interactions between extracardiac regulatory mechanisms (autonomous, hemodynamic, and endocrine) (28–30). However, in a previous study, we demonstrated that beat rate variability (BRV) in cardiac cell cultures (representing an in vitro model of a spontaneously active network of coupled cells) also follows a power law behavior in the absence of any extrinsic regulatory mechanisms (31). This suggests that not only extracardiac influences but also mechanisms intrinsic to cardiac tissue contribute to the power law behavior of HRV observed in vivo. Within an isolated network of pacemaker cells, BRV might be determined by the complex nonlinear dynamics of interactions among a large number of cell oscillators. However, it might also be determined by the integration of stochastic phenomena occurring at the cellular level.

To gain deeper insight into the phenomena underlying the power law behavior of HRV, our study pursued the following aims: 1), to analyze the spatiotemporal patterns of spontaneous electrical activity on a beat-to-beat basis in cultures of neonatal rat ventricular myocytes, 2), to assess whether spontaneous activity in these cultures shares ionic mechanisms similar to those in the SAN, and 3), to investigate, using mathematical modeling of SAN cells and networks, whether stochastic phenomena occurring at the cellular level may contribute to beating variability and/or explain the characteristics of BRV. Specifically, we sought to determine the effects i), of fluctuations of transmembrane currents (as caused by the stochastic gating of sarcolemmal channels), ii), of the stochastic gating of  $\text{Ca}^{2+}$  release channels in the sarcoplasmic reticulum (SR), and iii), of the dynamic turnover of ion channels in the cell membrane.

## MATERIALS AND METHODS

### Patterned growth cardiomyocyte cultures on microelectrode arrays

Monolayer cultures and patterned disk-shaped cultures of neonatal rat ventricular myocytes (Wistar; 1–2-day old; Zentrale Tierställe, University of

Bern, Bern, Switzerland) were prepared and grown on microelectrode arrays (Sensors, Actuators and Microsystems Laboratory, University of Neuchâtel, Neuchâtel, Switzerland) following previously published photolithographic procedures (31–33). Dissociated ventricular myocytes were preplated for 2 h in culture flasks to reduce the percentage of nonmyocardial cells. Before seeding the dissociated myocytes, the microelectrode arrays were mounted in custom-fabricated chambers (diameter 12.3 mm; volume 1 ml), incorporating a connection interface for the microelectrode arrays. The cardiomyocytes were seeded at a density of 1600–2100 cells/mm<sup>2</sup>. The preparations were incubated at 36°C and 0.9% CO<sub>2</sub> in medium 199 with Hanks' salts (M-199, Sigma-Aldrich, Buchs, Switzerland) supplemented with 5% neonatal calf serum (Bioconcept, Allschwil, Switzerland), penicillin (20,000 units/L; Fakola, Basel, Switzerland), streptomycin (34  $\mu\text{mol/L}$ ; Fakola), vitamin B12 (15  $\mu\text{mol/L}$ ; Sigma-Aldrich), bromodeoxyuridine (100  $\mu\text{mol/L}$ ; Sigma-Aldrich), and epinephrine (10  $\mu\text{mol/L}$ ; Sigma-Aldrich).

### Recording of extracellular electrograms

Electrophysiology experiments were performed in 3–4-day-old cultures (31). Before an experiment, the culture medium was renewed. The chambers were then connected to a custom-designed amplifier array (gain: 1000 $\times$ ) and placed back into the incubator. A period of  $\geq 60$  min was allowed for equilibration of temperature ( $36.0^\circ\text{C} \pm 0.1^\circ\text{C}$ ). Control measurements of temperature using a thermocouple probe (Fluke 80TK, Wallisellen, Switzerland) were performed to verify that fluctuations of temperature were  $< 0.1^\circ\text{C}$  (peak-to-peak). Extracellular electrograms ( $V_e$ ) were recorded from an array of 61 indium-tin oxide microelectrodes (diameter 40  $\mu\text{m}$  each), arranged along a hexagonal lattice (layout shown in Fig. 1 A, inter-electrode distance (IED) = 1.425 mm). The amplified signals were sampled at 10 kHz (Data Acquisition Processor 4400a, Microstar Laboratories, Bellevue, WA) and analyzed using custom-written software.

### Data analysis

The data analysis methods used in this study are illustrated in Fig. 1. As illustrated in Fig. 1 B, activation times (i.e., times of occurrence of electrical activations at a given electrode) were defined as the times of occurrence of the minimum of the first derivative ( $dV_e/dt_{\min}$ ) of the extracellular electrograms (31). The accuracy of activation times' determination was investigated using computer simulations of synthetic signals and is presented in detail in the Supplementary Material. The large signal/noise ratio of the electrograms and the rapidity of the negative deflection (duration in the range 0.3–0.8 ms) permitted us to determine these fiducial points with a maximal absolute error of 0.15 ms (maximal standard deviation of the error  $< 0.1$  ms) without the need to filter the signals. The maximal error in the determination of interbeat intervals was thus double this value, i.e., 0.3 ms.

For every experiment, the acquired data and all fiducial markers of  $dV_e/dt_{\min}$  (detected automatically using a custom-written computer program) were carefully inspected visually and edited to ensure that all activations had been detected and to remove erroneous detections.

The top diagrams in Fig. 1, C and D, represent electrograms, fiducial markers, and corresponding isochrone activation maps for two successive beats. Isochrone maps were constructed based on triangulation and linear interpolation of the activation times corresponding to a given propagated action potential (34,35).

The origin of electrical activation, which we hereafter term "focus", was identified by a gradient-expansion iterative least squares surface fit of a hyperboloid function in the  $(x, y, t)$  space (Eq. 1 below) to the activation times  $t_{\text{act}}(x, y)$  using the Levenberg-Marquardt method (36,37):

$$((t_{\text{act}}(x, y) + \varepsilon - t_{\text{focus}})^2 - \varepsilon^2)\theta^2 = (x - x_{\text{focus}})^2 + (y - y_{\text{focus}})^2, \quad (1)$$

where  $\theta$  is conduction velocity at infinite distance from the focus,  $t_{\text{focus}}$  is the activation time at the focus,  $(x_{\text{focus}}, y_{\text{focus}})$  are the coordinates of the focus,

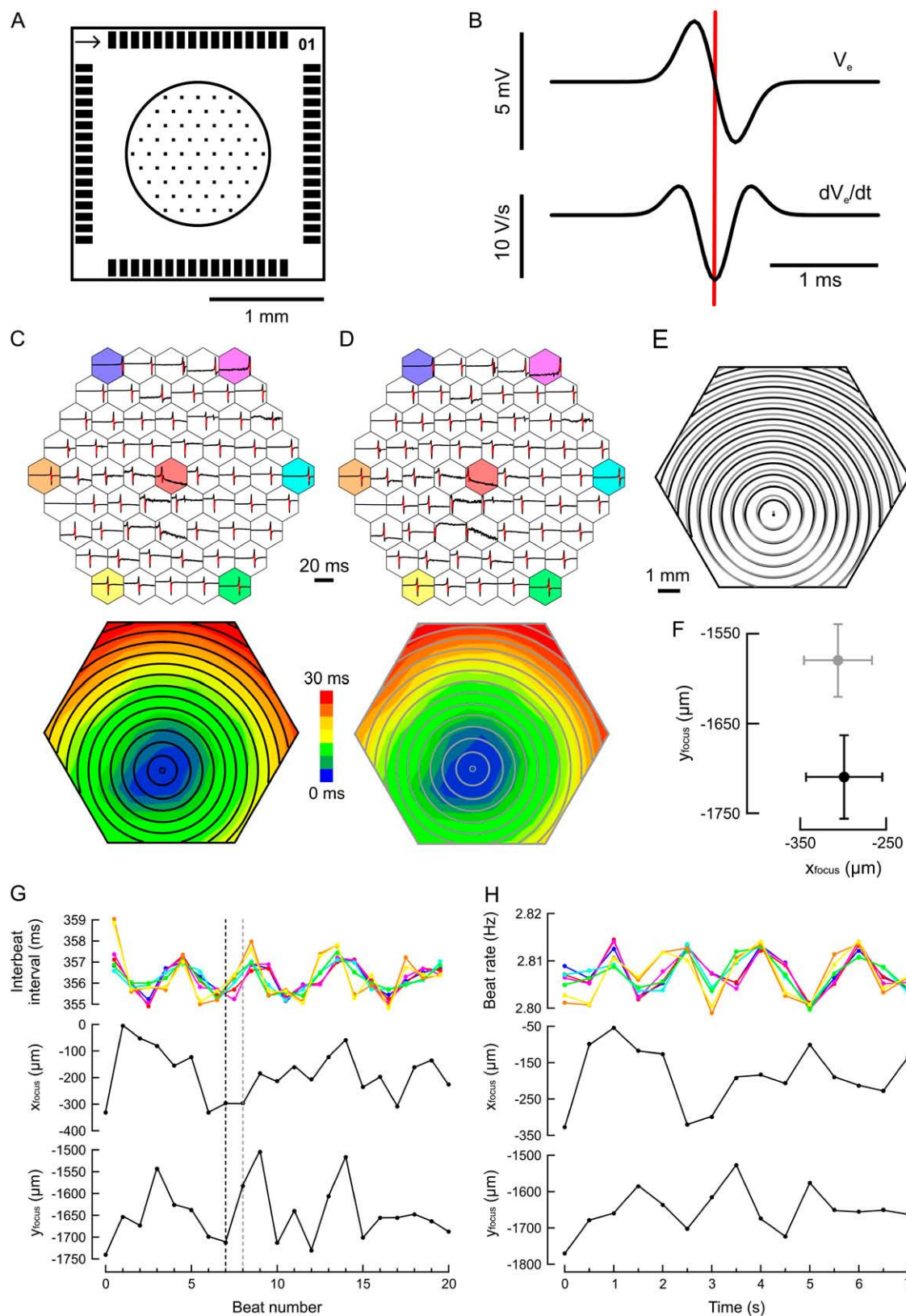


FIGURE 1 Recording of spontaneous activity of cardiac cell cultures and data analysis. (A) Microelectrode array layout. The dots indicate the positions of the microelectrodes. The circle denotes the culture area. (B) Representative extracellular electrogram ( $V_e$ ) recorded during spontaneous activity (top) and its first time derivative ( $dV_e/dt$ , bottom). The red line marks activation time (occurrence of  $dV_e/dt_{min}$ ). (C and D) Top: Signals recorded during two successive beats normalized to signal amplitude. Vertical red markers denote  $dV_e/dt_{min}$ . Bottom: Corresponding isochrone maps and localization of the focus of activation. The

and  $\varepsilon$  is the hyperbolic term (we observed that the least squares error is smaller and the fit more accurate if this term is included; if  $\varepsilon = 0$ , the function represents a cone in the  $(x, y, t)$  space). Because the cells were seeded on a uniform substrate, conduction velocity was assumed to be isotropic. This method to locate the focus is illustrated in Fig. 1, *C* and *D*, where isochrones based on this surface-fitting procedure are represented by concentric circles overlaid on the color-coded isochrone maps and where the central dots correspond to the identified foci. The least squares fits were assumed to be successful when the  $\chi^2$  test associated with the iteration process converged in  $<100$  iterations. Because this analysis was convergent only if enough operational electrodes were available for a reliable determination of activation times, we excluded experiments in which  $>50\%$  of the electrodes were not utilizable because of deficient connections or low signal/noise ratios. The number and location of the electrodes for which accurate focus localization was essential are described in the Supplementary Material.

To assess the applicability of Eq. 1 to describe the spread of focal activation, we computed the residuals between the measured activation times and the activation times fit with Eq. 1. We repeated this procedure for every focal activation in all experiments and applied the Kolmogorov-Smirnov test to evaluate whether the residuals differ from a Gaussian distribution. For all the focal activations analyzed, the hypothesis that the distributions of the residuals follow a normal distribution was never rejected (at  $p < 0.05$  level), indicating that Eq. 1 is adequate to describe the spread of focal activation. We also computed the correlation coefficient of the fit ( $r$ ), which was on average  $>0.99$ .

The two-dimensional (2-D) fits represented by circles in Fig. 1, *C* and *D*, are overlaid in Fig. 1 *E*. The fact that the two fitted maps are not concentric is suggestive of a displacement of the focus. Since conduction is never absolutely uniform in a biological preparation (even in a cell culture that is microscopically homogeneous) and since nonuniform conduction can affect the precision of the determination of  $x_{\text{focus}}$  and  $y_{\text{focus}}$ , we quantified conduction nonuniformity (CNU) and evaluated the influence thereof on the accuracy of focal point localization. The nonuniformity of conduction was reflected by the fact that the standard deviation of the residuals ( $SD_{\text{resid}}$ ) was in the range of a couple of milliseconds and thus several times larger than the precision of activation time determination (see above).

$SD_{\text{resid}}$  thus provides quantitative insight into CNU at the spatial scale corresponding to the resolution of the system ( $IED = 1.425$  mm). To quantify CNU at this scale, we computed the ratio between  $SD_{\text{resid}}$  and the time required by the wavefront to cover the IED (conduction time) as  $CNU = SD_{\text{resid}}/(IED/\theta)$ , where  $\theta$  is the conduction velocity obtained from the fit to Eq. 1 and  $IED/\theta$  corresponds to the expected conduction time. CNU is a unitless parameter (expressed as percentage) and can be interpreted as a coefficient of velocity variation. A similar method has been used previously to quantify CNU in cultured cell strands (38). In this study, CNU ranged from 6% to 20%.

$SD_{\text{resid}}$  was subsequently used to quantify the standard deviation of the fitted focus coordinates  $x_{\text{focus}}$  and  $y_{\text{focus}}$  (for details, see Press et al. (37)). The computed standard deviations of focus coordinates ( $SD_x$  and  $SD_y$ ), therefore, characterize the error in the localization of the focus, which is essentially due to the nonuniformity of conduction intrinsic to the biological preparations. In the two activations depicted in Fig. 1, *C* and *D*,  $SD_{\text{resid}}$  was 0.84 and 0.74 ms, CNU was 14.3% and 12.8%, and  $r$  was 0.9926 and 0.9938, respectively. As shown in Fig. 1 *F*,  $SD_x$  and  $SD_y$  amounted to 43

and 47  $\mu\text{m}$  for the beat illustrated in Fig. 1 *C*, and to 38 and 40  $\mu\text{m}$  for the beat depicted in Fig. 1 *D*, for which the computed focus location shifted by 130  $\mu\text{m}$ .

The determination of  $SD_x$  and  $SD_y$  was verified and validated by Monte Carlo simulations of synthetic data sets (37) in which a perturbation having a normal distribution with a standard deviation equal to  $SD_{\text{resid}}$  was added to the fitted activation times at each electrode. These simulations confirmed the computed  $SD_x$  and  $SD_y$  with a precision of 1%. The statistical probability that focus coordinates were equal for the two beats depicted in Fig. 1, *C* and *D*, was  $p = 0.028$ . This example therefore illustrates the limit of our algorithm to discriminate between two different foci.

This analysis yielded similar results when applied on different beats in different experiments and thus shows that changes in computed focus position several times the spatial  $SD_x$  and  $SD_y$  can be considered significant, although much smaller than the spatial resolution of the microelectrode array. However, accurate assessment ( $SD_x$  and  $SD_y < 100 \mu\text{m}$ ) of the focus position was possible only when the focus was located within the area mapped by the electrodes and the algorithm permitted only an approximate localization when the focus was outside this area. To confirm that the system and the analysis algorithm are able to accurately identify the origin of focal electrical activation in monolayer cultures, we paced the preparations from defined locations. Subsequent analysis of the focus of activation pinpointed the centers of the stimulation electrodes with a precision of 50  $\mu\text{m}$  (see the Supplementary Material for details).

Fig. 1 *G* illustrates interbeat interval series for the six corner electrodes and the center electrode as well as focus coordinates for 20 successive beats. Interbeat interval variations (in the range of milliseconds) were significantly larger than the maximal error of their determination (0.3 ms). The crossing of the different traces reflects the movement of the focus on a beat-to-beat basis.

Beat rate (BR) and the PSD of BRV were computed as described previously (31), using established methods applied for the frequency domain analysis of HRV in vivo (4). In brief, evenly sampled series (2 Hz) of instantaneous BR were constructed by linear interpolation from the series of activation times, as shown in Fig. 1, *G* and *H*. The PSD of BRV was then computed from the fast Fourier transform of the resampled BR series of one electrode. The power law exponent of the PSD was computed as the slope of the linear regression of  $\log(\text{PSD})$  versus  $\log(\text{frequency})$ . The discrete Fourier PSD data points were given a weight inversely proportional to their density on the logarithmic abscissa (31). A power law was assumed to be present if  $r > 0.85$ . Similarly, evenly sampled series (2 Hz) of focus coordinates (see Fig. 1, *G* and *H*) were constructed by linear interpolation and were used to compute and characterize the power spectra of these coordinates.

## Experimental protocols

The preparations were inspected using phase contrast microscopy to verify their structural intactness (i.e., uniformity of cell density, absence of localized damage). Structurally nonuniform preparations were discarded.

Experiments in which the spatiotemporal characteristics of beating variability were investigated were conducted in disk-shaped cultures (diameter: 11 or 12.3 mm) after enhancing sustained spontaneous electrical activity with 0.4  $\mu\text{mol/L}$  Bay K 8644 (31). After an equilibration period of  $\geq 60$  min, the electrical activity was recorded continuously for 30 min. To verify that

FIGURE 1 (Continued)

hexagon denotes the area mapped by the electrodes. The colored map is based on triangulation and linear interpolation of activation times. The overlaid solid (*C*) and shaded (*D*) circles represent isochrones (interval: 2 ms) based on the surface fit described by Eq. 1. The central dot denotes focus position based on this fit. (*E*) Overlay of the fitted maps for the beats shown in *C* (solid) and *D* (shaded). (*F*) Fitted focus coordinates (origin at the center of the array) and computed standard deviations  $SD_x$  and  $SD_y$  (error bars) determined based on the standard deviation of the residuals for the spontaneous activations shown in *C* (solid) and *D* (shaded), respectively (see Materials and Methods for details concerning the analysis). (*G*) Top: Interbeat interval series (20 successive beats) for the corner and central electrodes (colors corresponding to *C* and *D*). Bottom: Corresponding focus coordinates. Solid and shaded dashed lines mark the beats depicted in *C* and *D*, respectively. (*H*) Evenly resampled time series (2 Hz; used for spectral analysis), corresponding to the data shown in *G*.

fluctuations of temperature do not contribute to BRV under our recording conditions, control experiments ( $n = 5$  different cultures) were performed to evaluate what temperature difference ( $\Delta T$ ) is needed to produce a given change in BR ( $\Delta BR$ ). In these experiments, electrical activity and temperature were continuously recorded and temperature was increased from 34°C to 38°C and decreased from 38°C to 34°C by modifying the set point of the incubator. The sensitivity of BR to temperature, determined as  $\Delta BR/BR_{\text{average}}/\Delta T$  during the linear phases of temperature change, amounted to  $5.1\% \pm 1.7\%/^{\circ}\text{C}$  (range 2.3–7.5%/°C). In the other experiments presented in this study, BR variations were in the range of 2.5% and occurred rapidly over timescales of a few seconds. If they had been caused by temperature changes, such BR variations would have necessitated fast temperature variations in the range of 0.5°C. Thus, the contribution of temperature fluctuations (measured to be  $<0.1^{\circ}\text{C}$  in the incubator) to BRV was minimal.

Experiments in which the effect of pharmacological agents (nifedipine (Sigma-Aldrich), Bay K 8644, ryanodine, or ZD7288 (Tocris, Bristol, United Kingdom)) on BR was tested were performed on monolayer cultures covering the entire area at the bottom of the chambers. After a control recording (10 min), the compounds were added using a custom-built injection setup. Their effect on BR was assessed by comparing BR during 10-s periods immediately before and 1.5 min after injection, respectively. Control experiments were performed with vehicle medium to verify that the injection itself did not induce significant modifications of BR. The injection led to a minimal decrease in BR by  $2\% \pm 1\%$  ( $n = 4$ ), possibly caused by a slightly lower temperature of the injected vehicle.

## Mathematical modeling of pacemaker cells and networks

The Wilders-Jongsma-van Ginneken (WJvG) model of the rabbit SAN cell (39) was used to simulate the electrical activity of spontaneously active cells and cell networks. The model takes into account 10 transmembrane currents, intracellular compartmentation, and changes of  $[\text{Na}^+]_i$ ,  $[\text{K}^+]_i$ , and  $[\text{Ca}^{2+}]_i$  in different compartments. In cell networks, intercellular gap junctional conductance was set to 2.58 nS, following values reported previously (40).

Membrane potential, gating variables of ion currents, and ion concentrations were integrated explicitly using a constant time step ( $dt$ ) of 0.005 ms. Activation times were defined for every cell as the time when membrane potential reached  $-30$  mV during depolarization. In the networks, focus position was defined for every activation as the location of the earliest activated cell.

## Stochastic fluctuations of transmembrane current

The effects of fluctuations of transmembrane current due to stochastic open-close kinetics of ion channels was investigated by introducing into the model a fluctuation current,  $I_{\text{fluct}}$ , with zero mean and no long-term correlations.  $I_{\text{fluct}}$  was constructed as a stochastic Ornstein-Uhlenbeck process (41) by iteration of the following equation:

$$I_{\text{fluct}}(t + dt) = I_{\text{fluct}}(t) - \beta I_{\text{fluct}}(t)dt + \sigma(2\beta dt)^{0.5}\xi(t), \quad (2)$$

with  $\beta$  the rate constant determining the extent of temporal correlations,  $\sigma$  the standard deviation of the fluctuation current, and  $\xi(t)$  a normally distributed random variable with zero mean and unitary standard deviation. We set  $\beta = 0.7 \text{ ms}^{-1}$ , which resulted in  $I_{\text{fluct}}$  with an autocorrelation function that decreased below 0.05 for time lags  $>4$  ms. This reflects the notion that ion channels remain open for a few milliseconds and have no long-term memory of their history of conformational states.

## Stochastic gating of ryanodine receptors

To test the contribution of the stochastic open-close kinetics of the SR  $\text{Ca}^{2+}$  release channels (ryanodine receptors (RyRs)) to beating variability, we

modified the original formulation of the  $\text{Ca}^{2+}$  release current,  $I_{\text{rel}}$ , in the WJvG model given as (39)

$$I_{\text{rel}} = A_{\text{rel}}[\text{Ca}^{2+}]_{\text{Rel}}/[1 + (K_{\text{m,Ca}}/[\text{Ca}^{2+}]_i)^2] \quad (3)$$

by the following formulation:

$$I_{\text{rel}} = A_{\text{rel}}P_{\text{o,RyR}}([\text{Ca}^{2+}]_{\text{Rel}} - [\text{Ca}^{2+}]_i), \quad (4)$$

with  $P_{\text{o,RyR}}$  the fraction of open RyRs,  $[\text{Ca}^{2+}]_{\text{Rel}}$  the  $\text{Ca}^{2+}$  concentration in the release store,  $[\text{Ca}^{2+}]_i$  the myoplasmic  $\text{Ca}^{2+}$  concentration,  $A_{\text{rel}}$  the maximal permeability (permeability of all RyRs together), and  $k_{\text{m,Ca}}$  the binding constant of myoplasmic  $\text{Ca}^{2+}$  to RyRs. The term  $([\text{Ca}^{2+}]_{\text{Rel}} - [\text{Ca}^{2+}]_i)$  represents the  $[\text{Ca}^{2+}]$  difference between the release store and the myoplasm. The gating of individual RyRs and thus the fraction of open RyRs ( $P_{\text{o,RyR}}$ ) was computed as a stochastic Markov process following a two-state model with a second-order dependence on  $[\text{Ca}^{2+}]_i$ . Following Sobie et al., we incorporated a constant closing rate,  $\beta$ , of  $0.5 \text{ ms}^{-1}$  (42). The  $\text{Ca}^{2+}$  dependence of the opening rate,  $\alpha$ , was formulated as

$$\alpha = \beta([\text{Ca}^{2+}]_i/K_{\text{m,Ca}})^2. \quad (5)$$

At steady state (constant  $[\text{Ca}^{2+}]_i$ ),  $P_{\text{o,RyR}}$  is thus  $\alpha/(\alpha + \beta) = 1/[1 + (K_{\text{m,Ca}}/[\text{Ca}^{2+}]_i)^2]$  and corresponds to the third term of the original  $I_{\text{rel}}$  formulation. Following Bers (43), we assumed a number of 5000 RyR channels in a cell (number required to attain a typical peak  $[\text{Ca}^{2+}]_i$  during  $\text{Ca}^{2+}$ -induced release in a cell having the volume of the WJvG cell (5 pL)). At each time step  $dt$  of the simulations (satisfying  $\alpha dt$  and  $\beta dt \ll 1$ ), for each closed RyR (respectively, open RyR), one random number,  $A$ , was drawn from the uniform distribution  $[0,1]$ . If  $A < \alpha dt$  (respectively,  $A < \beta dt$ ) then the channel was opened (respectively, closed).

## Ion channel turnover

Incorporation of channels into the plasma membrane and their internalization from the membrane (turnover) were formulated as a stochastic “immigration-death” model, in which the incorporation and the internalization of channels were formulated as Poisson processes (41) for the two principal ion channel types of the WJvG model, the L-type  $\text{Ca}^{2+}$  channels, and the delayed rectifying  $\text{K}^+$  channels.

The processes were formulated based on the average number,  $N_{\text{average}}$ , of channels in the plasma membrane (10,000 and 1000, respectively (44)) and the half-lives of the channels (16 and 4 h, respectively (45)). If  $t_{1/2}$  is the half-life of a given type of channel, then the recycling rate ( $\delta$ ) is related to  $t_{1/2}$  by  $\delta = (\ln 2)/t_{1/2}$ . To maintain  $N_{\text{average}}$  channels in the membrane, channels must therefore be incorporated at a rate,  $\alpha$ , which is  $N_{\text{average}}$  times larger, i.e.,  $\alpha = \delta N_{\text{average}}$ .

At each time step,  $dt$ , of the simulation (satisfying  $\alpha dt$  and  $\delta dt \ll 1$ ) for each cell and for each channel type, one random number,  $A$ , was drawn from the uniform distribution  $[0,1]$ . If  $A < \alpha dt$  then one channel was incorporated. Then, for each individual channel, one random number,  $B$ , was drawn from the uniform distribution  $[0,1]$ . If  $B < \delta dt$  then the channel was removed from the cell membrane.

## Statistics

Values are given as mean  $\pm$  SD. Data were compared using the Wilcoxon signed rank test or the Student's  $t$ -test, and  $p < 0.05$  was considered significant.

## RESULTS

### Origin of spontaneous activity in disk-shaped cultures

To characterize the patterns of spontaneous activity in the neonatal rat cardiomyocyte cultures, we first investigated

whether this activity originates from foci located at preferential locations. Sustained activity was induced in disk-shaped monolayer cultures by application of Bay K 8644 ( $0.4 \mu\text{mol/L}$ ) and recorded during 30-min periods using the electrode layout shown in Fig. 2 *A*. In 11 out of 12 different preparations, the activity was of focal origin, as illustrated by the isochrone maps shown in Fig. 2, *B* and *C*. In one experiment, spontaneous activity was due to reentry of the action potential.

When a focal activation originated within the hexagonal area covered by the electrodes (e.g., Fig. 2 *B*), focus position could be reliably assessed (see Materials and Methods). However, when the focus was outside this limit (e.g., Fig. 2 *C*), focus position could not be evaluated with satisfactory precision. This concerned 17% of all activations in all 11 experiments.

In the analysis presented in Fig. 2 *D*, the culture area was divided into concentric regions in which the density of focus occurrences was calculated (i.e., the relative number of occurrences divided by the area of the corresponding region). This analysis, covering >96,000 focal activations in 11 different cultures, revealed a largest density of focus occurrences in the paracentral regions (*b* and *c*) and in the periphery of the preparations (*f*). These two maxima were, however, not significantly different.

### Spatiotemporal analysis of beating variability in disk-shaped cultures

In a former study, we showed that BRV in the monolayer cultures exhibits a power law behavior with fractal features in the temporal domain, similar to HRV in vivo (31). We extended this study with the analysis of beating variability in

the spatial domain by quantifying changes in focus position on a beat-to-beat basis.

Because the precise extrapolation of focus position beyond the area mapped by the electrodes was not possible, we conducted this analysis on 5 out of 11 experiments in which the focus remained in the hexagonal mapping area during the entire duration of the recording.

This analysis is illustrated in Fig. 3 for one experiment in a disk-shaped culture (Fig. 3 *A*) exhibiting focal activity (isochrone map and focus identification in Fig. 3 *B*). Instantaneous BR (Fig. 3 *C*) exhibited an aperiodic pattern of variability, as shown by the absence of peak in the PSD of BRV (Fig. 3 *D*). The linear aspect of the spectrum on the double logarithmic scale reveals the power law behavior of BRV. The power law exponent was  $-1.40$ , corresponding to the slope of the regression line. In Fig. 3 *E*, the beat-to-beat movement of the focus is illustrated by the trajectory interconnecting successive focus positions. The movement of the focus was irregular, exhibiting not only slow drifts and excursions but also more abrupt position changes. We computed the maximal focus excursion, defined as the largest distance between all foci identified during the 30-min recording. This maximal excursion, i.e., the largest focus displacement, was 2.78 mm and was thus orders of magnitude larger than the accuracy of focal point localization.

Inspection at different magnifications of the geometrical object formed by the set of focus positions suggests that this set exhibits a scale-independent fractal aspect. The fractal box dimension of this set, computed following Peitgen et al. (16), was 1.58. The movement of the focus is further illustrated in Fig. 3 *F*. The 30-min recording was segmented into 90 bins of 20 s each, and the median as well as the range (minimum to maximum) of the *x* and *y* coordinates are

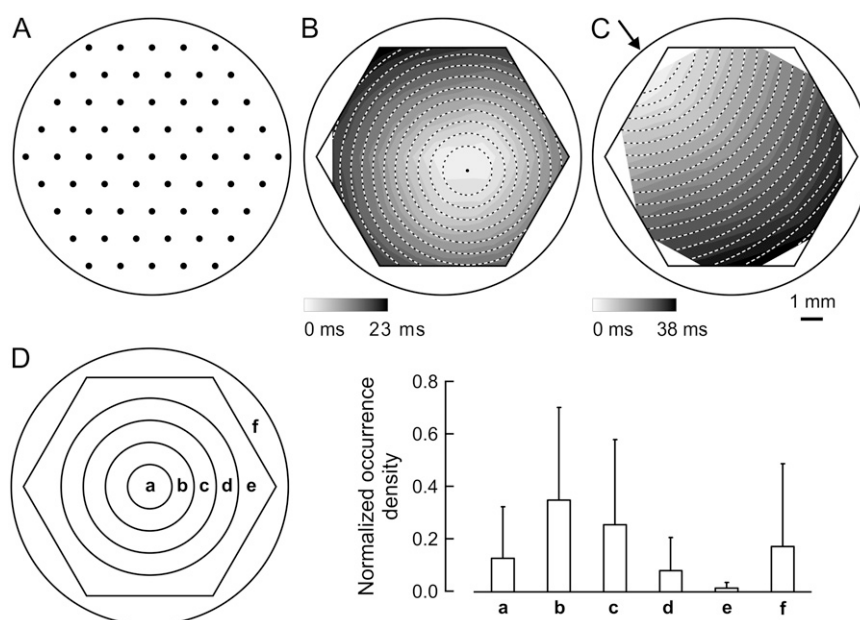
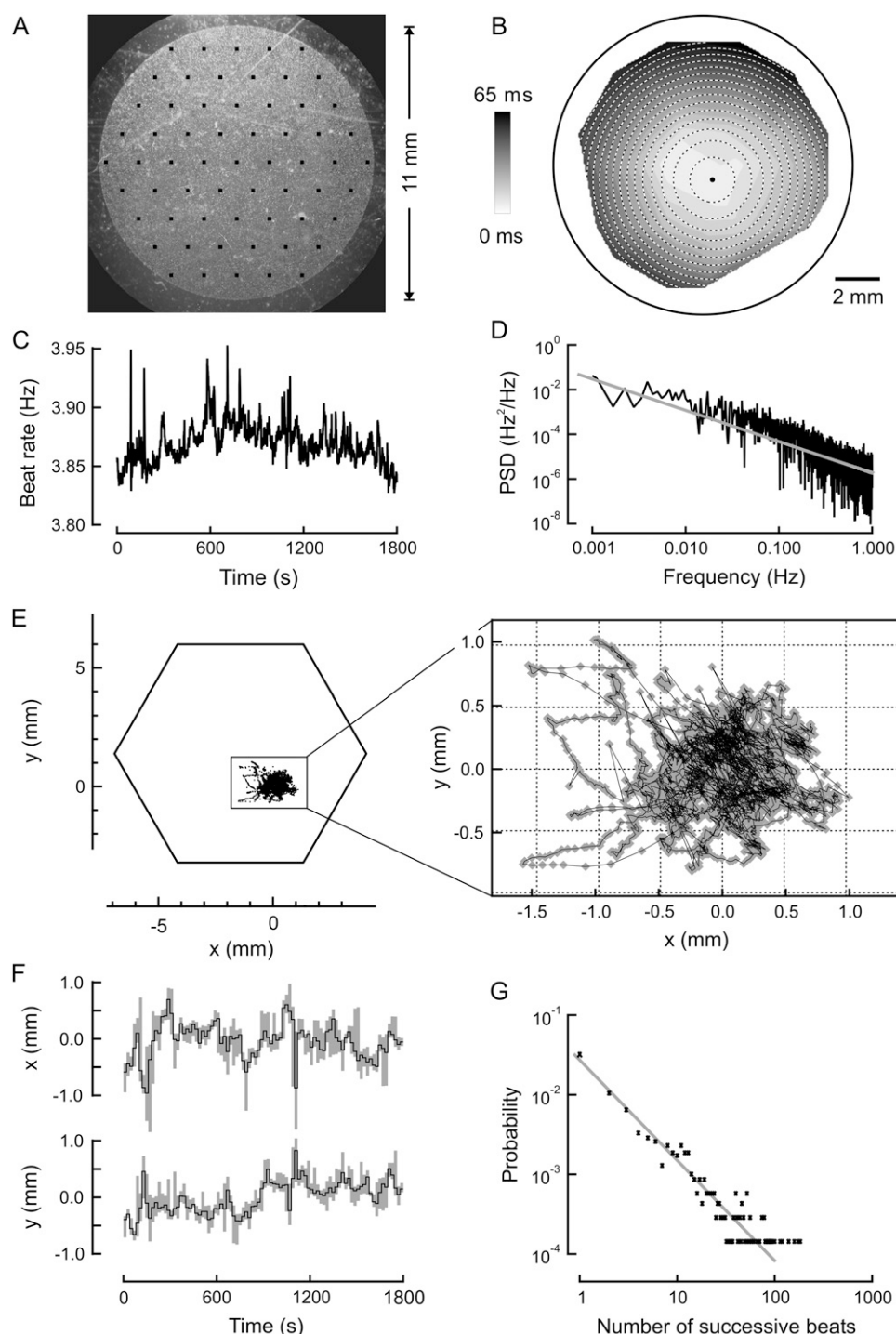


FIGURE 2 Origin of focal activity in disk-shaped monolayer cultures of neonatal rat cardiomyocytes. (A) Layout of the recording electrodes (hexagonal lattice, marked with dots). The circle denotes the culture area. (B) Isochrone map of a focal activation originating within the hexagonal mapping area. The grayscale map was constructed by linear interpolation and the concentric circles by surface fitting (interval: 2 ms); the focus is marked by the solid dot. (C) Map of an activation originating beyond the hexagonal limit (arrow). (D) Histogram of focus occurrence density in the regions labeled *a–f* in the schematic ( $n = 11$  different cultures).



**FIGURE 3** Spatiotemporal analysis of beating variability in a disk-shaped monolayer culture of neonatal rat ventricular myocytes. (A) Photograph of the preparation. The recording sites are marked with dots. (B) Isochrone map of an activation. The grayscale map was constructed by linear interpolation and the concentric circles by surface fitting (interval: 4 ms); the focus is marked by the solid dot. (C) BR as a function of time. Note the aperiodic variations of BR. (D) PSD of BRV. The spectrum was characterized by a power law (regression line in the double logarithmic plot) with an exponent of  $-1.40$ . (E) Left: Map illustrating the continuously varying position of the focus (dots) during the 30-min recording. The hexagon denotes the mapping area. Right: Magnification of the object formed by the ensemble of focus positions (shaded symbols) and the trajectory of the focus (interconnecting line). (F) Focus coordinates (axes shown in E) as a function of time, illustrating the irregular movement of the focus. The recording was segmented into 20-s bins. The solid line marks the median value for each bin, and the shaded band represents the range (minimum to maximum) for the corresponding bins. (G) Residence time distribution of the focus, i.e., distribution of the number of successive times a focus remained within a given square domain (grid illustrated in E) before moving to another. The residence time distribution followed a power law function with an exponent of  $-1.26$ .

shown for every bin as a function of time. The data show the presence of slow focus drifts occurring over timescales of minutes. To evaluate the behavior of focus position in the frequency domain, we conducted a Fourier analysis of these coordinates. Similar to BRV in the temporal domain, the PSDs of the coordinates (not shown) were characterized by a power law with exponents of  $-1.58$  and  $-1.59$  for the  $x$  and  $y$  coordinates, respectively.

We also described the dynamics of focus movement by evaluating during how many successive beats the focus remains at or close to a given location, thus giving indications about how frequently the focus moves to a remote location. For this purpose, we segmented the  $x$ - $y$  plane into a grid with a given mesh size ( $0.49 \times 0.49$  mm in Fig. 3 E) and counted the number of successive times the focus remained within a given grid segment before moving to another. The



histogram in Fig. 3 *G* illustrates the normalized distribution of this “residence time” (hereafter termed “residence time distribution”). The residence time distribution also followed a power law function with an exponent of  $-1.26$ . We repeated this analysis using different mesh sizes and observed that the distribution always followed a power law behavior for mesh sizes 0.3–1.4 mm (not shown).

Altogether, these analyses reveal that beating variability displays an aperiodic scale-independent fractal behavior not only in the temporal domain (i.e., concerning BRV) but in the spatial domain as well (i.e., concerning the origin of activation). Individual fractal measures and surface fit parameters characterizing the uniformity of conduction and accuracy of focus determination are presented in Table 1 for the five preparations investigated. In all five preparations, these analyses yielded similar results. In the temporal domain, BRV was characterized by a power law behavior with an average exponent of  $-1.38 \pm 0.14$  (consistent with our previous study (31)). In the spatial domain, the fractal box dimension of focus trajectory was  $1.42 \pm 0.22$ . The average power law exponents of the spectra of focus coordinates were  $-1.40 \pm 0.16$  and  $-1.35 \pm 0.15$  for  $x$  and  $y$ , respectively, without statistical difference between them (consistent with the symmetry and isotropy of the preparations). The average power law exponent of the residence time distribution (mesh size: 0.49 mm) was  $-1.69 \pm 0.41$ . The exponents of the power law behavior of BRV of focus coordinates and of the residence time distribution were all in a similar range, and no correlation was found between them.

Furthermore, no correlation was observed between BR and focus position, indicating that a given BR is not linked to

the presence of the focus at a specific location. To evaluate whether abrupt changes in focus position were linked to abrupt changes in BR, we also computed the cross correlation between the series of absolute beat-to-beat differences in BR and the series of beat-to-beat displacements of the focus. The cross correlation exhibited a small peak of  $0.20 \pm 0.04$ , present in all five experiments. This suggests that an abrupt change in focus position might, to a small extent, be associated with an abrupt change in BR, but the poor correlation indicates that focus shifts are certainly not the only mechanism underlying BR changes.

### Pharmacological investigation of depolarizing mechanisms underlying the spontaneous electrical activity in cardiomyocyte cultures

In the SAN, it is well known that the L-type  $\text{Ca}^{2+}$  current  $I_{\text{Ca,L}}$ , the  $\text{Na}^+/\text{Ca}^{2+}$  exchange current  $I_{\text{NCX}}$  consecutive to spontaneous  $\text{Ca}^{2+}$  release from the SR, and the hyperpolarization-activated cation current  $I_f$  are the major contributors to phase 4 depolarization (46–48). However, in cultures of neonatal rat ventricular myocytes, the ionic mechanisms underlying spontaneous depolarization and generation of electrical activity have not been fully characterized.

Here we used a pharmacological approach to evaluate the contribution of these depolarizing currents to spontaneous activity in the cardiomyocyte cultures.  $I_{\text{Ca,L}}$  was blocked or increased using nifedipine or Bay K 8644, correspondingly. Ryanodine and ZD7288 were used to block  $\text{Ca}^{2+}$  release from the SR ( $I_{\text{rel}}$ ) and  $I_f$ , respectively. In all these experiments, the activity was always of focal origin.

**TABLE 1** Surface fit and culture parameters

Preparation	A	B	C	D	E	Mean $\pm$ SD
Surface fit parameters						
$r$	.9900 $\pm$ .0122	.9980 $\pm$ .0013	.9979 $\pm$ .0012	.9783 $\pm$ .0050	.9904 $\pm$ .0065	.9909 $\pm$ .0072
SD <sub>resid</sub> (ms)	0.82 $\pm$ 0.33	0.41 $\pm$ 0.08	3.62 $\pm$ 0.06	1.16 $\pm$ 0.11	3.25 $\pm$ 0.63	1.85 $\pm$ 1.32
Standard deviation of coords. ( $\mu\text{m}$ )	42 $\pm$ 21	40 $\pm$ 11	25 $\pm$ 6	58 $\pm$ 7	72 $\pm$ 14	48 $\pm$ 16
CNU (%)	11.2 $\pm$ 4.5	9.3 $\pm$ 1.8	7.7 $\pm$ 1.2	19.7 $\pm$ 1.6	14.3 $\pm$ 2.9	12.4 $\pm$ 4.3
Culture parameters						
Mean BR (Hz)	3.28	2.43	3.81	3.10	3.87	3.30 $\pm$ 0.53
$\beta$ BRV	-1.39	-1.18	-1.58	-1.36	-1.40	-1.38 $\pm$ 0.14
$\beta_x$	-1.31	-1.56	-1.25	-1.27	-1.58	-1.40 $\pm$ 0.16
$\beta_y$	-1.37	-1.34	-1.21	-1.27	-1.59	-1.35 $\pm$ 0.15
Box dimension	-1.60	-1.44	-1.05	-1.45	-1.58	-1.42 $\pm$ 0.22
$\beta$ RTD	-1.62	-2.37	-1.50	-1.69	-1.26	-1.69 $\pm$ 0.41
Max. excursion (mm)	3.22	2.15	2.42	4.52	2.78	3.02 $\pm$ 0.83

$r$ : correlation coefficient of surface fit.

SD<sub>resid</sub>: standard deviation of residuals.

standard deviation of coords.: standard deviation of fitted focus coordinates.

CNU conduction nonuniformity: see Materials and Methods.

Mean BR: mean beat rate.

$\beta$  BRV: power law exponent of beat rate variability.

$\beta_x$ ,  $\beta_y$ : power law exponents of coordinates' variability.

$\beta$  RTD: power law exponent of residence time distribution.

Max. excursion: maximal focus excursion.

Data presented in Fig. 3 were obtained from preparation E.



Although 38% of preparations (16 out of 42) exhibited spontaneous activity (BR;  $2.46 \pm 1.04$  Hz), most preparations were quiescent (62%). As shown in Fig. 4 A, nifedipine ( $5 \mu\text{mol/L}$ ) silenced the beating of cultures that were active. Conversely, Bay K 8644 ( $0.4 \mu\text{mol/L}$ ) markedly increased BR. Moreover, the application of Bay K 8644 initiated spontaneous activity in all the cultures that were initially quiescent.

Because only a small fraction of our preparations was spontaneously active, we tested the modulation of BR by ryanodine and ZD7288 in the presence of Bay K 8644 ( $0.4 \mu\text{mol/L}$ ). Under these conditions, BR was  $5.10 \pm 0.58$  Hz. Ryanodine is known to produce a biphasic effect on RyRs: at submicromolar concentrations, it increases the permeability of the SR to  $\text{Ca}^{2+}$ , whereas micromolar concentrations increase the closed state probability of the channel (49). As illustrated in Fig. 4 B, we observed a corresponding concentration-dependent effect: at a concentration of  $10 \mu\text{mol/L}$ , ryanodine strongly reduced BR in all experiments. However, BR was always accelerated when a lower concentration of ryanodine was used ( $0.1 \mu\text{mol/L}$ ). The  $I_f$  blocker ZD7288 ( $100 \mu\text{mol/L}$ ) slightly reduced BR.

These experiments were paralleled with computer simulations using the WJvG cell model by scaling the corresponding conductances or permeabilities. As shown in Fig. 4 C, the simulations resulted in qualitatively similar changes in BR. However, the dependence of BR on  $I_{\text{Ca,L}}$  was smaller in comparison with the changes observed in the cultures. BR exhibited a monotonic dependence on the total permeability of RyRs, and a reduction of  $I_{\text{rel}}$  always resulted in a decrease of BR. Finally, BR decreased to a similar extent when  $I_f$  conductance was reduced.

In the cell model, we also investigated the effects of changes in the maximal conductance of the delayed rectifier  $\text{K}^+$  current  $I_K$  (Fig. 4 C). The sensibility of BR on  $I_K$  density was prominent, in particular for decreased  $I_K$  conductance, which led to a marked reduction of BR.

### Theoretical investigation of BRV induced by transmembrane current fluctuations

Voltage-gated currents are mediated by conformational changes of ion channels (e.g., openings and closings) in response to membrane potential changes. The ensemble current carried by channels of a given type is characterized by an average response to a given modification of membrane potential (e.g., a given voltage-clamp protocol or the action potential itself). However, the behavior of individual channels of the same type is different, because their conformational changes occur in a stochastic manner (50). This stochastic behavior will lead to beat-to-beat differences between the actual current and the average response. These deviations will vary from beat-to-beat and will also be different for distinct cells during their excitation by the same action potential.

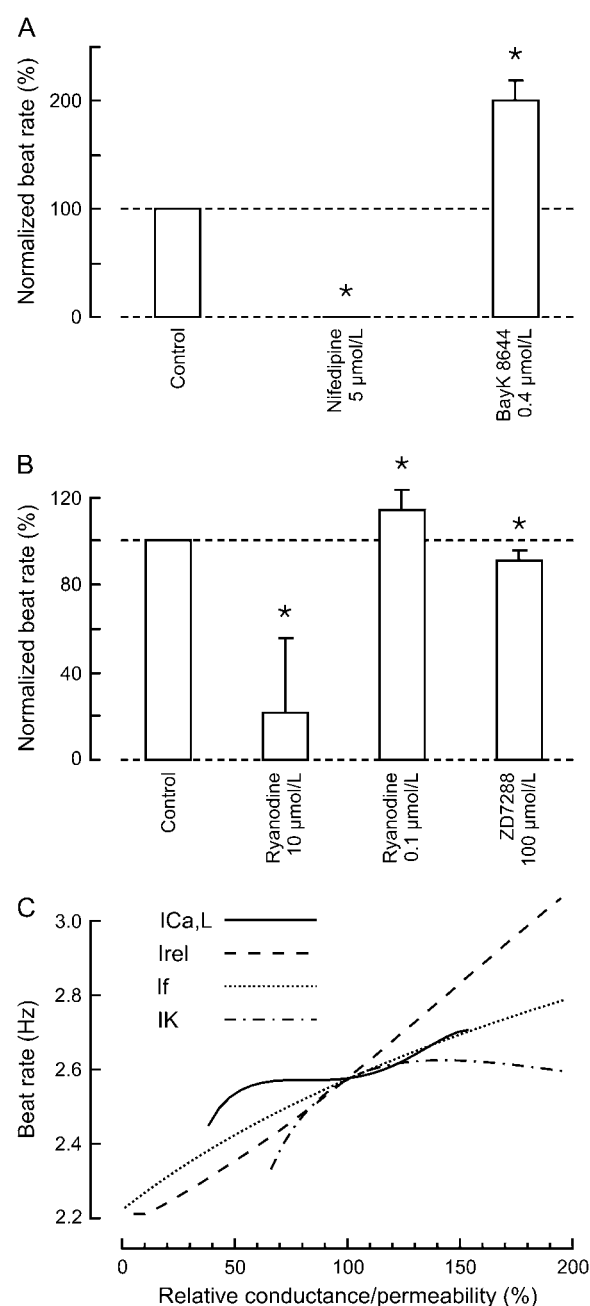


**FIGURE 4** Effects of pharmacological interventions targeting ion transport on the rate of spontaneous focal activity in monolayer cultures of neonatal rat ventricular cells. (A) Whereas nifedipine silenced the preparations ( $n = 6$ ), Bay K 8644 strongly enhanced spontaneous activity ( $n = 12$ ). Asterisks indicate  $p < 0.05$  versus control. (B) In the presence of Bay K 8644 ( $0.4 \mu\text{mol/L}$ ), ryanodine ( $10 \mu\text{mol/L}$ ) depressed spontaneous activity ( $n = 6$ ), whereas at a lower concentration ( $0.1 \mu\text{mol/L}$ ), it slightly accelerated BR ( $n = 6$ ). ZD7288 slightly decreased BR ( $n = 6$ ). Asterisks indicate  $p < 0.05$  versus control. (C) Corresponding interventions simulated using the WJvG model by scaling the corresponding conductances/permeabilities. Interruptions of the curves indicate conditions under which spontaneous action potentials ceased or the cell failed to repolarize normally.

To evaluate the effects of such fluctuations in transmembrane current on beating variability, we introduced into the model a transmembrane fluctuation current,  $I_{\text{fluct}}$ , mimicking the beat-to-beat differences caused by this stochastic open-close behavior of channels (see Materials and Methods).

Fig. 5 *A* illustrates the behavior of a single model cell in which an  $I_{\text{fluct}}$  with a standard deviation of 0.162 pA/pF was introduced.  $I_{\text{fluct}}$  resulted in BRV exhibiting a flat power spectrum (absence of power law behavior). The standard deviation of BRV was 0.037 Hz. As shown in Fig. 5 *B*, the standard deviation of BRV was proportional to the standard deviation of  $I_{\text{fluct}}$ . Excessive  $I_{\text{fluct}}$  (SD > 2 pA/pF) resulted in large and unrealistic oscillations of membrane potential and a disruption of this linear relationship.

The effect of  $I_{\text{fluct}}$  on beating variability was then evaluated in a 2-D network of 156 WJvG cells (Fig. 5 *C*). The cells in the network were arranged into an octagonal shape, approximating the shape of a disk. Gap junctional coupling was homogeneous and constant within the network. The resulting spatiotemporal dynamics were very dissimilar to those observed in the experiments.  $I_{\text{fluct}}$  with a standard deviation of 0.162 pA/pF (as in Fig. 5 *A*) induced BRV with an ascending power spectrum. The power law exponent was thus positive (+0.71 in the example;  $+0.74 \pm 0.07$  in five different simulations). In the spatial domain, the focus exhibited frequent and large beat-to-beat changes. For almost every activation, the focus leaped over large distances (if represented, the trajectory of the focus would fill the entire network area). Accordingly, as shown by the residence time distribution, the probability that the focus remained at one

location for two or more successive beats was <5%. Furthermore, the residence time distribution was better fitted by an exponential than by a power law function. Interestingly, activations originated more frequently from the periphery of the network.

### Theoretical investigation of beating variability induced by stochastic open-close kinetics of RyRs

To evaluate the patterns of beating variability caused by variations in  $\text{Na}^+/\text{Ca}^{2+}$  exchange current due to the stochastic nature of  $\text{Ca}^{2+}$  release events from the SR (51), the deterministic formulation of the average behavior of RyRs was replaced by a stochastic two-state gating model of individual RyR channels (see Materials and Methods).

In a single cell, as shown in Fig. 6 *A*, stochastic RyR gating led to fluctuations in the  $\text{Na}^+/\text{Ca}^{2+}$  exchange current ( $I_{\text{NCX}}$ ) and to corresponding variations in the rate of phase 4 depolarization ( $dV/dt$ ). The  $dV/dt$  variations resulted in BRV (BR:  $2.521 \pm 0.011$  Hz). However, the power spectrum of BRV was flat, indicating the absence of a power law behavior of BRV.

In the cell network (Fig. 6 *B*, same network as in Fig. 5 *C*), stochastic RyRs gating led to BRV (BR:  $2.522 \pm 0.003$  Hz) with a spectrum that had a positive power law exponent ( $+0.14 \pm 0.12$  in five different simulations). The spatial characteristics of focus position (not shown) were similar to those induced by stochastic fluctuations in transmembrane current (in Fig. 5 *C*), with large and frequent beat-to-beat

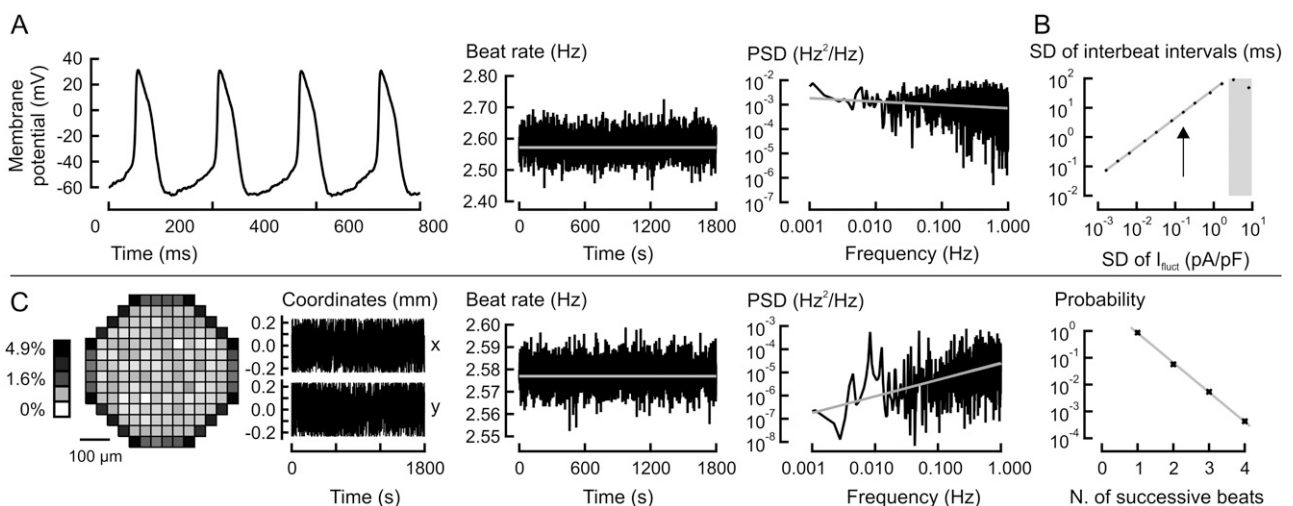


FIGURE 5 Beating variability induced by stochastic fluctuations of transmembrane current in a single model cell (*A* and *B*) and in a network of pacemaker cells (*C*). (*A*) Action potentials, BRV, and power spectrum of BRV in the model cell after introduction of fluctuations ( $I_{\text{fluct}}$ ) with a standard deviation of 0.162 pA/pF. The shaded line indicates BR in the absence of  $I_{\text{fluct}}$ . The spectrum was flat. (*B*) Standard deviation of interbeat intervals as a function of the standard deviation of  $I_{\text{fluct}}$ . The relationship is linear for  $I_{\text{fluct}}$  with standard deviation <2 pA/pF (slope of the regression line: 0.99). Larger  $I_{\text{fluct}}$  resulted in excessive perturbations of membrane potential (shaded area). The arrow corresponds to  $I_{\text{fluct}}$  used in *A* and *C*. (*C*) Map of focus occurrence, focus coordinates, BRV, PSD of BRV, and residence time distribution in the network. The spectrum exhibited an ascending behavior (positive power law exponent of +0.71). The residence time distribution was characterized by an exponential function (note the linear abscissa and the logarithmic ordinate).

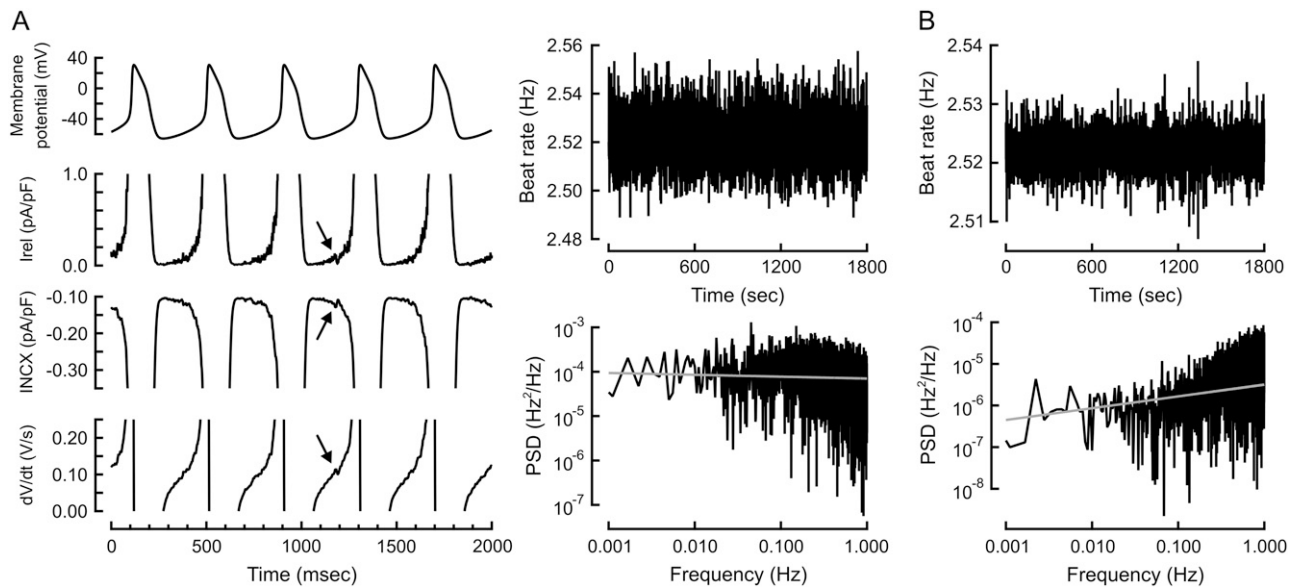


FIGURE 6 Beating variability induced by stochastic open-close kinetics of RyRs in a single model cell (A) and in a network of pacemaker cells (B; same network as in Fig. 5 C). (A) Left: Action potentials,  $\text{Ca}^{2+}$  release current ( $I_{\text{rel}}$ ),  $\text{Na}^{+}/\text{Ca}^{2+}$  exchange current ( $I_{\text{NCX}}$ ), and rate of rise of membrane potential during phase 4 depolarization ( $dV/dt$ ). Variations in  $I_{\text{rel}}$  caused by stochastic release events resulted in variations in  $I_{\text{NCX}}$  and modulated diastolic  $dV/dt$  (arrows). Right: BRV and its PSD in the single cell. The spectrum was flat (no power law). (B) BRV and its PSD in the cell network. The spectrum exhibited a power law with a positive exponent (+0.28, regression line, shaded).

changes in focus position, an exponential residence time distribution, and a preferential location of foci at the periphery of the network.

### Theoretical investigation of beating variability induced by ion channel turnover

In living cells, membrane proteins undergo an incessant turnover: synthesized membrane proteins are stored in transport vesicles and incorporated into the membrane. In parallel, membrane proteins are continuously internalized. This trafficking concerns ion channels as well (45). Because of the discrete nature of incorporation and internalization, the number of channels in a cell varies with time, and the average number of channels depends on the quantitative relation between the rates of synthesis/incorporation and recycling/degradation. Furthermore, distinct cells, being “on average identical”, may have different densities of channels at a given instant. The variation of ion current densities in space and in time might lead to variations in the rate of a spontaneously active network and in focus position.

The results presented in Fig. 4 indicate that  $I_{\text{Ca,L}}$  density plays a significant role in determining BR in both the cultures and the WJvG model. Previous studies indicate that BR of pacemaker cells also depends on the density of the delayed rectifier  $\text{K}^{+}$  current (46), a finding corroborated by the simulations shown in Fig. 4 C. Therefore, if channel turnover leads to beating variability, this variability should be principally caused by the turnover of these two types of channels.

We first investigated the dynamics of ion channel turnover and its influence on beating variability in a single model cell. We formulated incorporation and recycling of ion channels as independent Poisson processes, based on the average number of channels of these two types and their corresponding half-lives reported in the literature (see Materials and Methods). Fig. 7 illustrates the variation of the number of channels in a cell and its consequence on BRV.

The left panel of Fig. 7 A illustrates different simulations of the variation of the number  $N(t)$  of delayed rectifier  $\text{K}^{+}$  channels with an expected (average) value  $N_{\text{average}}$  of 1000 channels. The histogram of  $N(t)$  followed a Poisson distribution with a mean equal to its variance (i.e., 1000) and thus a standard deviation of  $N_{\text{average}}^{0.5} = 31.6$  and a coefficient of variation ( $\text{SD}/N_{\text{average}}$ ) of 3.16% (corresponding to  $N_{\text{average}}^{-0.5}$ ). The right-hand panel illustrates the variability of  $N(t)$  in the frequency domain. The power spectrum of  $N(t)$  followed a power law with an exponent of  $-2$  (which is characteristic of Brownian noise), flattening out at frequencies  $<10^{-5}$  Hz. Similarly, Fig. 7 B illustrates the variability of the number of L-type  $\text{Ca}^{2+}$  channels. Because of the larger  $N_{\text{average}}$  (10,000), the standard deviation of  $N(t)$  was larger (100) but the coefficient of variation was smaller (1%). Fig. 7 C depicts the effect of the variation of the number of  $\text{K}^{+}$  and  $\text{Ca}^{2+}$  channels on the BR of the WJvG model cell. BR varied between 2.54 and 2.59 Hz. Because of the relatively larger variability in  $\text{K}^{+}$  current density, BR was essentially linked to the number of  $\text{K}^{+}$  channels and was less influenced by the number of  $\text{Ca}^{2+}$  channels. In the frequency domain, BRV followed a power law behavior with an

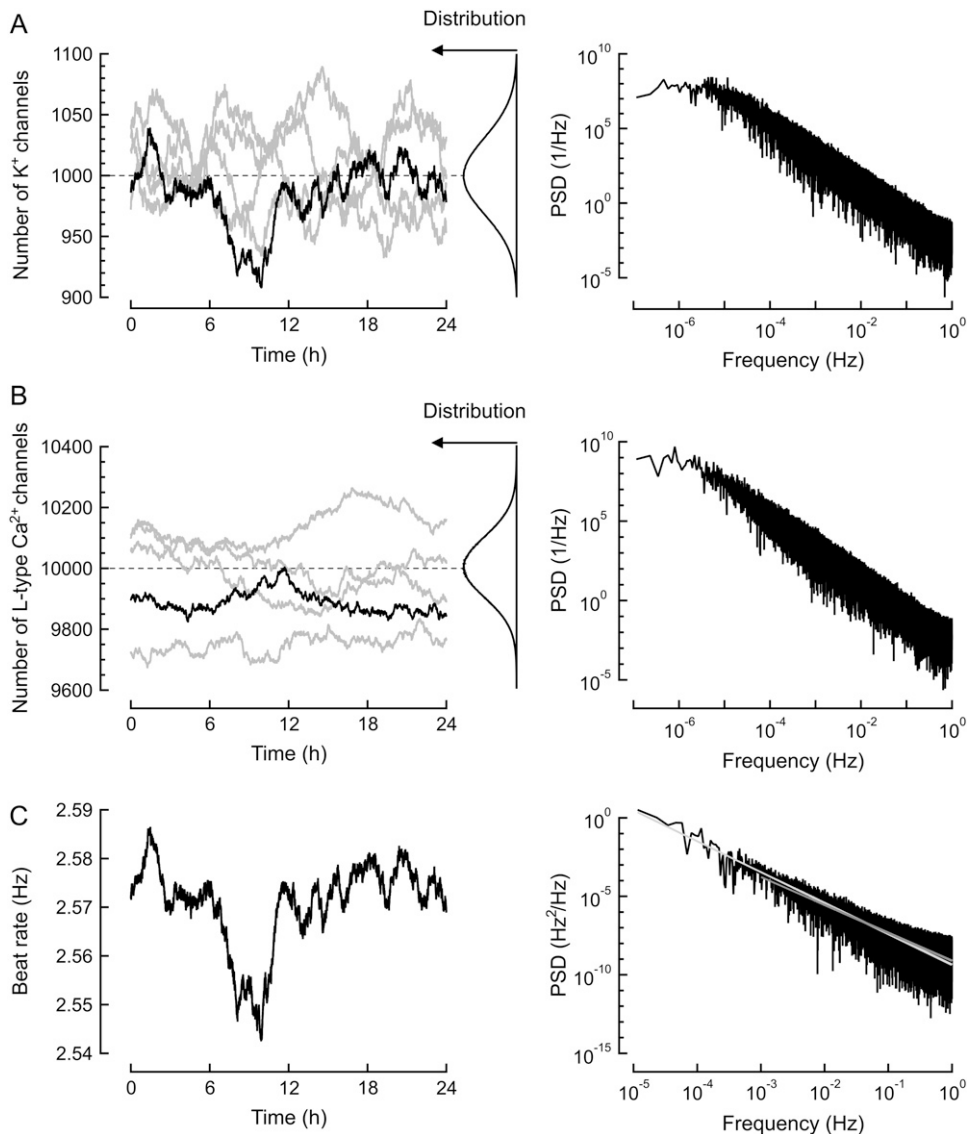


**FIGURE 7** Model of ion channel turnover and effects of the turnover of delayed rectifier  $K^+$  channels and L-type  $Ca^{2+}$  channels on BR in a single cell. (A) Left: Variation of the number of delayed rectifier  $K^+$  channels, with a channel half-life of 4 h and an average number of 1000 channels. The turnover process is illustrated for five different 24-h periods. The number of channels followed a Poisson distribution (shown on the right). Right: Power spectrum of the variation of the number of channels. The spectrum followed a power law with an exponent of  $-2$  and flattened for frequencies  $<10^{-5}$  Hz. (B) Turnover of L-type  $Ca^{2+}$  channels, with a channel half-life of 16 h and an average number of 10,000 channels. Same layout as in A. (C) Left: BRV in a single cell induced by the variations highlighted in A and B. Because the relative variation of the number of  $K^+$  channels  $SD/mean = 3.16\%$  was larger than that of the number of L-type  $Ca^{2+}$  channels (1%), BR was principally determined by the number of  $K^+$  channels. Right: The power spectrum of BRV followed a power law behavior. Over the range  $10^{-5}$ –1 Hz, the exponent was  $-1.97$  (light regression line). However, the spectrum was less steep for frequencies  $>10^{-3}$  Hz (exponent of  $-1.78$  in the range  $10^{-3}$ –1 Hz, darker regression line).

exponent of  $-1.95 \pm 0.03$  ( $n = 5$  simulations), corresponding to that of the variability of the number of channels. Interestingly, in the range  $10^{-3}$ –1 Hz, the slope of the spectrum was less steep ( $-1.82 \pm 0.03$ ,  $n = 5$ ).

The contribution of the turnover of these two channel types to beating variability was then evaluated in a 2-D network of 156 WJvG cells (see Fig. 8, same network as in Fig. 5 C). Introduction of channel turnover led to BRV around the nominal frequency of the WJvG cell (Fig. 8 A). In the frequency domain, these variations were characterized by a power law behavior (Fig. 8 B) with an exponent of  $-1.53$ . In the spatial domain, activity was of varying focal origin, as illustrated in Fig. 8, C and D. The residence time distribution (Fig. 8 E) followed a power law function with an exponent of  $-1.69$ . The beat-to-beat movement of the focus ( $x$  and  $y$  coordinates as a function of time) is illustrated in Fig. 8 F. Fourier analysis of these coordinates revealed an absence of periodic behavior and the PSD of the coordinates followed a

power law behavior with exponents of  $-1.21$  and  $-1.36$  for the  $x$  and  $y$  coordinates, respectively.

Similar characteristics were observed in five other simulations. In the temporal domain, BRV followed a power law behavior with an exponent,  $\beta$ , of  $-1.52 \pm 0.20$ , a value significantly different from the exponent observed in a single model cell (see Fig. 7). However, this exponent was not significantly different from that observed experimentally. In the spatial domain, the power law exponent of the coordinates spectra was  $-1.35 \pm 0.15$  (pooled values for  $x$  and  $y$ ). The power law exponent of the residence time distribution was  $-1.57 \pm 0.14$ .

### Effects of network dimensionality and size on the power law exponent $\beta$

The finding that the exponent  $\beta$  is different in single cells versus cellular networks indicates that the power law

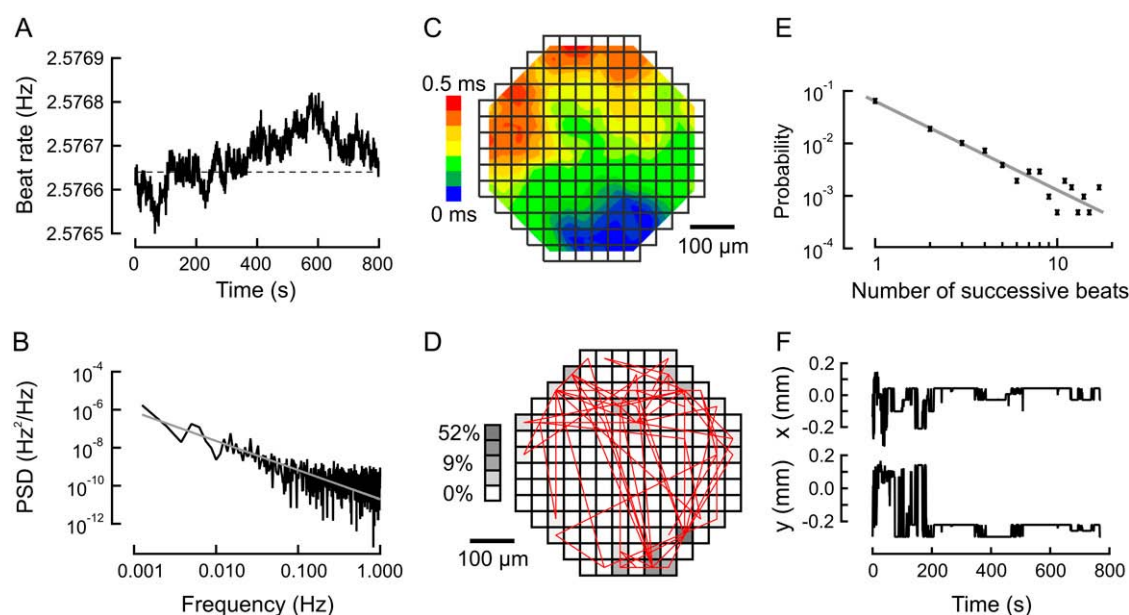


FIGURE 8 Spatiotemporal characteristics of beating variability in a network of WJvG model cells with turnover of L-type  $\text{Ca}^{2+}$  and delayed rectifier  $\text{K}^{+}$  channels. (A) BR of the network (layout in C and D). The dotted line indicates BR in the absence of channel turnover. (B) PSD of BRV. The exponent of the power law was  $-1.53$ . (C) Isochrone map of an activation. (D) Map illustrating the relative occurrence of the focus in different cells of the network. The line connects successive focus positions. (E) Residence time distribution. The distribution followed a power law (exponent of  $-1.69$ ). (F) Focus coordinates (origin at the center of the network), illustrating the irregular focus movement.

characteristics of BRV are influenced by intercellular interactions. These interactions are likely to be determined by both the dimensionality (i.e., one, two, or three dimensions) and the size of the network. Therefore, we investigated the effects of network dimensionality and size on the exponent  $\beta$ , as presented in Fig. 9.

First, as shown in Fig. 9 A,  $\beta$  was assessed in one-, two-, and three-dimensional (1-D, 2-D, and 3-D) symmetrical networks having approximately the same number of cells (incorporating ion channel turnover). The 1-D network consisted of a strand of 156 cells. The 2-D network was the same 156-cell network as depicted in Figs. 5 and 8 (diameter of  $\sim 14$  cells). The 3-D network was constructed to present a

3-D symmetry as shown in Fig. 9 A and consisted of 179 cells (diameter of  $\sim 7$  cells). Interestingly,  $\beta$  was least negative in the 1-D network ( $-1.31 \pm 0.21$ ,  $n = 5$ ) and most negative in the 3-D network ( $-1.68 \pm 0.09$ ,  $n = 5$ ). Because the 3-D network had the smallest diameter, its elements interacted over shorter distances. To test how dimensionality affects the power law behavior in networks of similar diameters, simulations were performed in symmetrical 1-, 2-, and 3-D networks each built with a different number of cells (7, 37, and 179, respectively) but all having a diameter of  $\sim 7$  cells. As shown in Fig. 9 B, for networks having a similar diameter, increasing network dimension led to less negative  $\beta$ . These results therefore suggest that  $\beta$  depends in a

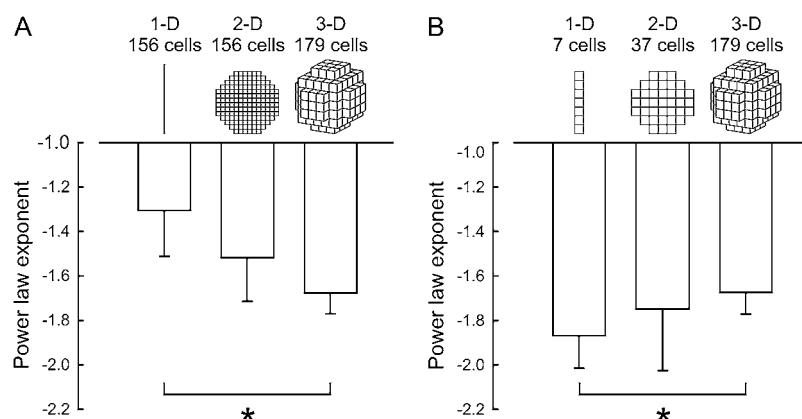


FIGURE 9 Effects of network dimensionality and size on the power law exponent. (A) Power law exponent as a function of dimension in symmetrical networks of approximately the same size. (B) Power law exponent as a function of dimension in networks of approximately the same diameter (seven cells). Asterisks denote significant differences ( $n = 5$ ).

complex manner on both network size and dimensionality and that the exponent  $\beta$  may even be closer to  $-1$  in large 3-D networks.

## DISCUSSION

Under our experimental conditions, spontaneous activity in cultures of densely seeded neonatal rat ventricular myocytes originates from a mobile focus and spreads radially across the entire tissue. The generation of this rhythm is a highly dynamic process and is based on ionic mechanisms also involved in the generation of the sinoatrial rhythm. The variability of both BR and of focus position is aperiodic, and the respective power spectra exhibit power law behavior. The numerical simulations suggest that these characteristics cannot be accounted for by “white noise” in the biological system, e.g., by fluctuations of transmembrane currents or stochastic release of calcium from intracellular stores. Rather, they necessitate the presence of mechanisms exhibiting correlations occurring over a broad range of temporal scales, e.g., as investigated in this study, the number of channels in the cell membrane.

### Mechanisms of beating variability

In a previous study, Wilders et al. modified their original SAN cell model (which we used in the theoretical part of this work) by incorporating a detailed formulation of the stochastic gating of all individual ion channels (44). Their model mimicked the irregular beating observed experimentally in isolated SAN cells. Stochastic channel gating led to uncorrelated interbeat intervals. A similar study was conducted by Guevara and Lewis (52), supporting the notion that the stochastic behavior of a population of channels could contribute to irregular beating. The spatiotemporal patterns of beating variability in cell networks were, however, not addressed in these studies.

To address the question of whether modulation of BR caused by stochastic ion channel gating may lead to the power law behavior of BRV, we incorporated into the model a transmembrane fluctuation current with temporal correlations that did not extend beyond the intrinsic beating period of the cell. This resulted in BRV with a flat power spectrum and thus an absence of correlations in the interbeat interval series, equivalent to the result of Wilders and Jongsma (44). We opted for this approach because long-term simulations incorporating the stochastic gating of every channel in every cell of the network would have been computationally prohibitive.

The application of  $I_{\text{fluct}}$  in the cell network resulted in a power law exponent of BRV of the network that became clearly positive, indicating that the intercellular interactions in the network act as a “high-pass filter”, attenuating preferentially the slow variations in BR. A similar result was

observed for different intensities of  $I_{\text{fluct}}$  and for  $I_{\text{fluct}}$  formulated as Gaussian white noise (not shown).

The fact that  $\text{Ca}^{2+}$  release from the SR (in the form of  $\text{Ca}^{2+}$  sparks) is strongly involved in the modulation of BR both in SAN cells (47,53) and in our cultures (Fig. 4) motivated us to investigate how the stochastic nature of  $\text{Ca}^{2+}$  release may contribute to BRV. Although we used a formulation of  $\text{Ca}^{2+}$  release that does not account for the sub-cellular features of the release system, our result nevertheless suggests that BRV induced by the stochastic opening of RyRs is characterized by an absence of temporal correlations. Accordingly, the spatiotemporal characteristics of beating variability were similar as those induced by fluctuations of transmembrane current.

Thus, the stochastic gating of sarcolemmal ion channels or of RyRs represent unlikely candidates to explain the characteristics of beating variability and the power law of BRV observed in the experiments. Other possible biophysical, biological, or molecular mechanisms underlying beating variability can then be envisioned from the fact that every cell is a dynamic structure in which a continuous self-rearrangement and numerous regulatory processes concerning all constitutive elements of the cell take place. Variations in cellular characteristics can concern all biochemical processes (concentrations of metabolites and signaling molecules; concentrations and activity of enzymes) and therefore the regulation of the biophysical properties of ion transporters (e.g., by phosphorylation or expression of different isoforms, circadian rhythms) (54). There is, however, no experimental approach that would permit a tight control of all these parameters at the cellular level and thus an experimental investigation of their involvement in beating variability. Furthermore, there is to date no mathematical model of a pacemaker cell that incorporates the details of biochemical reactions or molecular mechanisms in conjunction with the electrical function of the cell. Moreover, in electrophysiological models published to date (whether incorporating a deterministic or a stochastic approach to channel gating), the maximal conductances of ion currents, i.e., the number of channels, is considered to be time invariant.

To obtain insight into the electrophysiological consequences of one aspect of cellular self-rearrangement, we challenged this notion of invariance and developed an original formulation for the turnover of ion channels in which the number of channels results from the integration of isolated incorporation/removal events. The turnover of ion channels introduced longer time constants (several hours) into the WJvG model, leading to longer term fluctuations in the simulations. The temporal dynamics of the number of channels followed a time course characteristic of Brownian motion with long-term correlations and with a power law exponent of  $-2$ , which, at the single cell level, resulted in a power law behavior of BRV with an exponent in this range. In the 2-D 156-cell network, the high-pass filtering properties of the network then reduced the spectrum slope to values

close to  $-1.5$ , similar to those observed experimentally. This result suggests that it is necessary to consider phenomena characterized by long time constants and/or long-term correlations to explain the power law behavior of BRV. Nevertheless, the amplitudes of the variations of BR were notably smaller than those observed in the cultures, indicating that ion channel turnover alone cannot account for the full intensity of variability in the cultures.

Intuitively, one could explain the high-pass filtering effect by the fact that the network adapts itself to a change in intrinsic frequency of a particular cell. Because this adaptation takes a certain time (possibly depending on the position of the cell within the network), the network can more easily accommodate slower than faster variations of the intrinsic beating rate of individual cells. This easier accommodation to slower changes may then contribute to a stronger attenuation of low-frequency variations and a weaker attenuation of high-frequency components.

In our experiments, the variability of focus position was characterized by a power law behavior similar to that of BRV, a characteristic that was closely reproduced by the model incorporating the turnover of ion channels. This reflects the fact that action potentials are not initiated at random positions but focus position is related to the previous history of spontaneous activity. This memory of the previous history of focus position can be inferred from the residence time distributions. If focus positions were completely uncorrelated from beat-to-beat (corresponding, e.g., to blind throws of an object onto a grid with a probability,  $a$ , to hit a given grid segment), then the probability of having  $N$  successive occurrences at the same position would follow an exponential distribution of the type  $a^{-N}$ . The power law behavior of the residence time distributions indicates that, compared to an exponential distribution, the probability of having  $N$  successive occurrences at the same position is relatively higher for large  $N$  and relatively lower for small  $N$ , respectively. In other words, the longer the focus remains at or near a given location, the less likely it is to move to another location. Conversely, if the focus just moved to another location, it is relatively less probable that it will remain there. The presence of correlations extending over a broad range of temporal scales, i.e., an influence of the past history on the current dynamics, is also reflected by the behavior of focus position coordinates as a function of time.

Based on these considerations, we thus propose that the power law behavior of beating variability must be, at the level intrinsic to cardiac tissue, essentially caused by variations of cellular characteristics exhibiting long-term correlations. Ion channel turnover can represent a stochastic mechanism contributing to such variations of cellular characteristics. However, the largest part of variability probably emerges from variations (deterministic or stochastic) in biochemical or molecular processes involving the concentrations of enzymes, metabolites, and second messengers. For example, it has recently been shown that levels of cyclic adenosine 3',5'-

phosphate (cAMP), protein kinase A, phospholamban phosphorylation, and L-type  $\text{Ca}^{2+}$  channel phosphorylation are dynamically involved in the control of BR in SAN cells via modulation of  $\text{Ca}^{2+}$  cycling (55). The investigation of how these biochemical aspects are involved in beating variability was, however, beyond the extent of our study.

### Relationship between spatial and temporal dynamics

In the SAN, the origin of the spontaneous action potential is not static and changes according to the autonomic nervous tone. It has been shown that the site of initiation shifts in response to vagal stimulation (56,57) and that shifts in the site of origin correlate with changes in heart rate (58,59). However, our cultures are devoid of autonomous influences, and the correlation between focus shifts and changes in BR is negligible. This absence of correlation was also observed in the simulations, irrespective of the investigated mechanism of rate variability. Therefore, it is possible, as proposed previously, that the correlation present in the SAN is due to inhomogeneous vagal innervation and variable cell sensitivity to acetylcholine (60,61).

The SAN is often described as a population of electrically coupled pacemakers having different intrinsic frequencies. Their coordinated rhythm depends on the process of "mutual entrainment", which leads to a stable periodic behavior of the pacemaker cell network (62,63). In this situation, the BR of the SAN is the result of a "democratic" process underlying the coordinated firing of the SAN cells, with each cell contributing to the overall mutual entrainment (64). Moreover, the BR of the network and the focus of origin are not necessarily that of the intrinsically fastest pacemaker cell (65). The small or absent correlation between changes in focus location and sudden changes in BR in both the cultures and the mathematical model are thus not in discrepancy with this theory of synchronization.

### Ionic mechanisms of spontaneous focal activity

Since the development of techniques permitting the dissociation and culture of cardiac cells more than 40 years ago, it has been known that confluent cultures of ventricular myocytes beat spontaneously and synchronously (66,67). The ionic mechanisms underlying this automaticity have, however, never been dissected in detail.

The ability to generate spontaneous action potentials depends on the balance between inward and outward currents during subthreshold depolarization (phase 4), i.e., until membrane potential has reached a sufficient level permitting the activation of voltage-gated  $\text{Na}^+$  and/or  $\text{Ca}^{2+}$  currents. In a recent work, Pumir et al. report that blocking the time-independent  $\text{K}^+$  current  $I_{K1}$  with barium promotes spontaneous activity in cultures of ventricular myocytes (68). In this study, we investigated the contribution to



spontaneous beating of the principal depolarizing mechanisms known to contribute to the automaticity of SAN cells.

#### *Involvement of $I_{Ca,L}$ and RyRs*

Both the L-type  $Ca^{2+}$  current  $I_{Ca,L}$  and a functional  $Ca^{2+}$  release from the SR are essential for the establishment of focal activity in the cultures. The contribution of  $Ca^{2+}$  release through RyRs and of  $Na^+/Ca^{2+}$  exchange in the pacemaking process was previously demonstrated for SAN cells (48,69). This mechanism may thus also apply to cultured ventricular myocytes in which variations in intracellular  $Ca^{2+}$  concentration during phase 4 may modulate the total transmembrane current and therefore BR. The dual involvement of  $Ca^{2+}$  via  $I_{Ca,L}$  and RyRs suggests that the accelerating effect of the  $I_{Ca,L}$  agonist Bay K 8644 might be explained not only through its direct effect on  $I_{Ca,L}$ , but also by the increased influx of  $Ca^{2+}$  into the cell, which may increase the  $Ca^{2+}$  load in the SR and, in turn, promote the spontaneous release of  $Ca^{2+}$  from the SR (70).

#### *Involvement of $I_f$*

It was previously shown that the hyperpolarization-activated current  $I_f$  is present in cultures of neonatal rat ventricular myocytes with a midpoint of activation curve (71) which is close to their resting membrane potential (72). Furthermore, a recent study indicates that  $I_f$  is critical for spontaneous beating of neonatal rat cardiomyocytes (73).

We assessed the contribution of  $I_f$  by using the compound ZD7288 (74), an agent that has been shown to inhibit  $I_f$  and to lower the BR of pacemaker cells (75). In our experiments, the effect of this compound was moderate, suggesting that under our conditions,  $I_f$  plays only a modest role in the automaticity of the preparations. Possibly, the minimal diastolic potential might not reach values sufficiently negative that would allow  $I_f$  to activate to an extent large enough to become an important contributor to automaticity.

Altogether, these observations indicate that in cultures of ventricular myocytes,  $I_{Ca,L}$ ,  $I_f$ , and spontaneous  $Ca^{2+}$  release from the SR underlie pacemaking mechanisms that are also encountered in the SAN, the natural pacemaker of the heart.

### **Comparison with other studies**

In a previous study, Bub et al. investigated the spatiotemporal dynamics of spontaneous bursts of activity in cultures of chick embryonic ventricular myocytes using imaging of intracellular calcium concentration and modeled their results using a cellular automaton (76). They observed that bursts are initiated by a focal beat that does not propagate radially in all directions, but is subject to functional conduction block in one direction. Because of the unidirectional nature of this functional block, reentry of the action potential leads to the formation of spiral-shaped wavefronts underlying the burst

of activity, which then ceases spontaneously when the spiral tips (rotors) die out. The presence of spirals as a mechanism underlying spontaneous activity has also been proposed by Hwang et al. (77). In our experiments, however, focal beats always propagated in all directions without conduction block and initiation of reentry was never recorded (although, in one experiment, sustained reentrant activity was present from the beginning of the recording). This fundamental difference in dynamics is possibly related to the fact that our cultures were incubated in the presence of epinephrine, which increases  $I_{Ca,L}$  and gap junctional coupling, and to the use of Bay K 8644, an agent shown to decrease the probability of unidirectional conduction block in the setting of a mismatch between a small current source and a large load (78).

In another study, Pumir et al. studied the alterations of conduction patterns in rat ventricular myocyte cultures induced by the application of  $Ba^{2+}$  and of the gap junctional uncoupler heptanol (68). These interventions resulted in the fractionation of wavefronts and reentrant waves. Under control conditions they, however, report that spontaneous activity was focal ("pacemaker activity"), but the spatiotemporal dynamics of focal activity were not further investigated.

### **Limitations of the study**

The presented experiments were conducted on cultures of ventricular cells, which do not reproduce the same repertoire of ionic currents and the electrophysiology of SAN cells. Monolayer cultures of SAN cells would be ideal for this study. Although techniques to culture isolated SAN cells have been developed by other laboratories (e.g., Marvin et al. (79)), the small number of cells that can be obtained from the SAN will not permit us to generate dense, uncontaminated, and confluent monolayer cultures of SAN cells. From our pharmacological dissection of depolarizing mechanisms, it nonetheless appears that spontaneous beating in the cultures shares several common mechanisms with the natural pacemaker of the heart and thus that our neonatal ventricular myocyte cultures may be applicable to investigating mechanisms of BRV.

There is at present no electrophysiological model of cultured neonatal rat ventricular myocytes available and the theoretical part of the study was performed using a SAN cell model. Although a previously published ventricular cell model could have been used instead, such a model would have had to be modified to exhibit spontaneous activity. This could have been achieved in numerous ways by manipulating different currents, for example, by reducing  $I_{K1}$  as previously done in the Luo-Rudy model (80). An adequate tuning of a ventricular model to match the cultured myocytes used in this study would therefore necessitate precise measurements of all ion currents. Furthermore, after seeding, cultured cells undergo changes in their degree of differentiation (81) and the expression of ion channels depends on the age of the animals used and the age of the culture (82,83),

which would render the development of such a model difficult. The development of such a model reproducing in detail the behavior of neonatal rat ventricular myocytes in culture was out of the scope of our study. Although it cannot be excluded that the results may be quantitatively different in a ventricular cell model, we believe that the choice of a SAN cell model rather than a ventricular cell model modified to produce spontaneous activity is more appropriate to address beating variability in the context of the mechanisms of HRV intrinsic to cardiac tissue.

During the culture procedure, the cells were seeded randomly on the substrate. Nonetheless, it cannot be excluded that the preparations were not strictly homogeneous, because the seeded cells are obtained from different regions of the ventricles known to express ion channels at different levels. Inhomogeneities might influence the spatiotemporal patterns of beating variability. Furthermore, recent work has shown that myofibroblasts are also present in the cultures. These myofibroblasts establish connections with the myocytes by gap junctions and exert an electrotonic action on the myocytes (84,85) which modulates BR (86). Clusters of myofibroblasts might then modulate spatiotemporal patterns of pacemaking as well.

Our formulation of ion channel turnover was based on the assumption that incorporation/internalization of a given channel is governed by Poisson processes. However, it cannot be excluded that channel turnover is governed by more intricate principles, which may lead to slopes,  $\beta$ , that are different from those we observed in the model. A refined formulation of ion channel turnover will need to await the results of biological studies focusing on this specific subject.

Finally, our preparations did not incorporate the intricate tridimensional structure of the SAN, which, as suggested by the simulations, is likely to influence the slope  $\beta$ .

## Implications and conclusions

An extensive body of work has demonstrated the existence of fractal and multi-fractal dynamics in heart rate time series (87–89), reflected by the power law behavior of HRV with a typical power law exponent of  $-1$ . These studies proposed nonlinear fractal analysis of HRV as investigative and diagnostic methods in a variety of pathological conditions (19,90). In parallel, nonlinear mathematical models have been developed to clarify the nonlinear aspects of HRV based on the complex interactions between regulatory mechanisms mediated by the two branches of the autonomic nervous system (30).

Although, undoubtedly, extracardiac influences determine the complex behavior of HRV, we demonstrate here the existence of mechanisms occurring at the tissue level that are likely to influence it. The patterns of HRV occurring in vivo will result from the integrative interaction of extracardiac and cellular mechanisms. A comprehensive understanding of the nonlinear aspects of HRV should therefore take into account

and incorporate both extracardiac determinants and cellular phenomena occurring within natural pacemakers.

## SUPPLEMENTARY MATERIAL

An online supplement to this article can be found by visiting BJ Online at <http://www.biophysj.org>.

We express our gratitude to Prof. Stephan Rohr for the design and support of the experimental setup, to Regula Flückiger Labrada for the preparation of the cultures, and to Prof. Hugues Abriel for his invaluable comments on this manuscript.

This study was supported by the Swiss National Science Foundation (grant 3100A0-100285 to J.P.K.) and by the project "Heart Remodeling in Health and Disease" of the Swiss University Conference.

## REFERENCES

1. Cohen, M. A., and J. A. Taylor. 2002. Short-term cardiovascular oscillations in man: measuring and modelling the physiologies. *J. Physiol. (Lond.)*. 542:669–683.
2. Lanfranchi, P. A., and V. K. Somers. 2002. Arterial baroreflex function and cardiovascular variability: interactions and implications. *Am. J. Physiol. Regul. Integr. Comp. Physiol.* 283:R815–R826.
3. Sztajzel, J. 2004. Heart rate variability: a noninvasive electrocardiographic method to measure the autonomic nervous system. *Swiss Med. Wkly.* 134:514–522.
4. Camm, A. J., M. Malik, J. T. Bigger, G. Breithardt, S. Cerutti, R. J. Cohen, P. Coumel, E. L. Fallen, H. L. Kennedy, R. E. Kleiger, F. Lombardi, A. Malliani, A. J. Moss, J. N. Rottman, G. Schmidt, P. J. Schwartz, and D. Singer. 1996. Heart rate variability: standards of measurement, physiological interpretation, and clinical use. *Circulation.* 93:1043–1065.
5. Malik, M. 1998. Heart rate variability. *Curr. Opin. Cardiol.* 13:36–44.
6. Jasson, S., C. Medigue, P. MaisonBlanche, N. Montano, L. Meyer, C. Vermeiren, P. Mansier, P. Coumel, A. Malliani, and B. Swynghedauw. 1997. Instant power spectrum analysis of heart rate variability during orthostatic tilt using a time-/frequency-domain method. *Circulation.* 96:3521–3526.
7. Fagard, R. H., K. Pardaens, J. A. Staessen, and L. Thijs. 1998. Power spectral analysis of heart rate variability by autoregressive modelling and fast Fourier transform: a comparative study. *Acta Cardiol.* 53: 211–218.
8. Malliani, A., M. Pagani, and F. Lombardi. 1994. Physiology and clinical implications of variability of cardiovascular parameters with focus on heart rate and blood pressure. *Am. J. Cardiol.* 73:3C–9C.
9. Hilz, M. J., and M. Dutsch. 2006. Quantitative studies of autonomic function. *Muscle Nerve.* 33:6–20.
10. Piepoli, M., and L. Bernardi. 1998. Influence of arterial baroreceptors on heart rate variability. *Med. Prin. Pract.* 7:81–95.
11. Pumpura, J., K. Howorka, D. Groves, M. Chester, and J. Nolan. 2002. Functional assessment of heart rate variability: physiological basis and practical applications. *Int. J. Cardiol.* 84:1–14.
12. Kobayashi, M., and T. Musha. 1982. 1/f fluctuations of heartbeat period. *IEEE Trans. Biomed. Eng.* 29:456–457.
13. Akselrod, S., D. Gordon, F. A. Ubel, D. C. Shannon, A. C. Berger, and R. J. Cohen. 1981. Power spectrum analysis of heart rate fluctuation: a quantitative probe of beat-to-beat cardiovascular control. *Science.* 213: 220–222.
14. Lombardi, F. 2000. Chaos theory, heart rate variability, and arrhythmic mortality. *Circulation.* 101:8–10.
15. Huikuri, H. V., T. H. Mäkilä, C. K. Peng, A. L. Goldberger, U. Hintze, and M. Moller. 2000. Fractal correlation properties of R-R

- interval dynamics and mortality in patients with depressed left ventricular function after an acute myocardial infarction. *Circulation*. 101: 47–53.
16. Peitgen, H. O., H. Jürgens, and D. Saupe. 1992. *Chaos and Fractals: New Frontiers of Science*. Springer-Verlag, New York.
  17. Bassingthwaite, J. B., L. S. Liebovitch, and B. J. West. 1994. *Fractal Physiology*. Oxford University Press, New York.
  18. Lewis, C. D., G. L. Gebber, P. D. Larsen, and S. M. Barman. 2001. Long-term correlations in the spike trains of medullary sympathetic neurons. *J. Neurophysiol.* 85:1614–1622.
  19. Bigger, J. T., R. C. Steinman, L. M. Rolnitzky, J. L. Fleiss, P. Albrecht, and R. J. Cohen. 1996. Power law behavior of RR-interval variability in healthy middle-aged persons, patients with recent acute myocardial infarction, and patients with heart transplants. *Circulation*. 93:2142–2151.
  20. Mäkilä, T. H., S. Hoiber, L. Kober, C. Torp-Pedersen, C. K. Peng, A. L. Goldberger, and H. V. Huikuri. 1999. Fractal analysis of heart rate dynamics as a predictor of mortality in patients with depressed left ventricular function after acute myocardial infarction. TRACE Investigators. TRAndolapril Cardiac Evaluation. *Am. J. Cardiol.* 83: 836–839.
  21. Huikuri, H., T. Mäkilä, K. Airaksinen, T. Seppanen, P. Puukka, I. Raiha, and L. Sourander. 1998. Power-law relationship of heart rate variability as a predictor of mortality in the elderly. *Circulation*. 97:2031–2036.
  22. Huikuri, H. V., and T. H. Mäkilä. 2001. Heart rate variability in ischemic heart disease. *Auton. Neurosci.* 90:95–101.
  23. Ribeiro, A. L. P., F. Lombardi, M. R. Sousa, M. V. Lins Barros, A. Porta, V. Costa Val Barros, M. E. D. Gomes, F. Santana Machado, and M. Otavio Costa Rocha. 2002. Power-law behavior of heart rate variability in Chagas' disease. *Am. J. Cardiol.* 89:414–418.
  24. Stein, P. K., P. P. Domitrovich, H. V. Huikuri, R. E. Kleiger, and C. Investigators. 2005. Traditional and nonlinear heart rate variability are each independently associated with mortality after myocardial infarction. *J. Cardiovasc. Electrophysiol.* 16:13–20.
  25. Willson, K., and D. P. Francis. 2003. A direct analytical demonstration of the essential equivalence of detrended fluctuation analysis and spectral analysis of RR interval variability. *Physiol. Meas.* 24:N1–N7.
  26. Penzel, T., J. W. Kantelhardt, L. Grote, J. H. Peter, and A. Bunde. 2003. Comparison of detrended fluctuation analysis and spectral analysis for heart rate variability in sleep and sleep apnea. *IEEE Trans. Biomed. Eng.* 50:1143–1151.
  27. Mahon, N. G., A. E. Hedman, M. Padula, Y. Gang, I. Savelieva, J. E. P. Waktare, M. M. Malik, H. V. Huikuri, and W. J. McKenna. 2002. Fractal correlation properties of R-R interval dynamics in asymptomatic relatives of patients with dilated cardiomyopathy. *Eur. J. Heart Fail.* 4:151–158.
  28. Ivanov, P. C., M. G. Rosenblum, C. K. Peng, J. Mietus, S. Havlin, H. E. Stanley, and A. L. Goldberger. 1996. Scaling behaviour of heartbeat intervals obtained by wavelet-based time-series analysis. *Nature*. 383: 323–327.
  29. Aoyagi, N., K. Ohashi, and Y. Yamamoto. 2003. Frequency characteristics of long-term heart rate variability during constant-routine protocol. *Am. J. Physiol. Regul. Integr. Comp. Physiol.* 285:R171–R176.
  30. Kotani, K., Z. R. Struzik, K. Takamasu, H. E. Stanley, and Y. Yamamoto. 2005. Model for complex heart rate dynamics in health and diseases. *Phys. Rev. E Stat. Nonlin. Soft Matter Phys.* 72:041904.
  31. Kucera, J. P., M. O. Heuschkel, P. Renaud, and S. Rohr. 2000. Power-law behavior of beat-rate variability in monolayer cultures of neonatal rat ventricular myocytes. *Circ. Res.* 86:1140–1145.
  32. Rohr, S., D. M. Schölly, and A. G. Kléber. 1991. Patterned growth of neonatal rat heart cells in culture. Morphological and electrophysiological characterization. *Circ. Res.* 68:114–130.
  33. Rohr, S., R. Fluckiger-Labrada, and J. P. Kucera. 2003. Photolithographically defined deposition of attachment factors as a versatile method for patterning the growth of different cell types in culture. *Pflugers Arch.* 446:125–132.
  34. Fast, V. G., and A. G. Kléber. 1993. Microscopic conduction in cultured strands of neonatal rat heart cells measured with voltage-sensitive dyes. *Circ. Res.* 73:914–925.
  35. Meiry, G., Y. Reisner, Y. Feld, S. Goldberg, M. Rosen, N. Ziv, and O. Binah. 2001. Evolution of action potential propagation and repolarization in cultured neonatal rat ventricular myocytes. *J. Cardiovasc. Electrophysiol.* 12:1269–1277.
  36. Marquardt, D. W. 1963. An algorithm for least-squares estimation of nonlinear parameters. *J. Soc. Ind. Appl. Math.* 11:431–441.
  37. Press, W. H., S. A. Teukolsky, W. T. Vetterling, and B. P. Flannery. 1992. *Numerical Recipes in C: The Art of Scientific Computing*. Cambridge University Press, Cambridge, UK.
  38. Rohr, S., J. P. Kucera, and A. G. Kléber. 1998. Slow conduction in cardiac tissue, I: Effects of a reduction of excitability versus a reduction of electrical coupling on microconduction. *Circ. Res.* 83:781–794.
  39. Wilders, R., H. J. Jongsma, and A. C. van Ginneken. 1991. Pacemaker activity of the rabbit sinoatrial node. A comparison of mathematical models. *Biophys. J.* 60:1202–1216.
  40. Anumonwo, J. M., H. Z. Wang, E. Trabka-Janik, B. Dunham, R. D. Veenstra, M. Delmar, and J. Jalife. 1992. Gap junctional channels in adult mammalian sinus nodal cells. Immunolocalization and electrophysiology. *Circ. Res.* 71:229–239.
  41. Cox, D. R., and H. D. Miller. 1965. *The Theory of Stochastic Processes*. Chapman & Hall, London.
  42. Sobie, E. A., K. W. Dilly, J. dos Santos Cruz, W. J. Lederer, and M. S. Jafri. 2002. Termination of cardiac  $\text{Ca}^{2+}$  sparks: an investigative mathematical model of calcium-induced calcium release. *Biophys. J.* 83:59–78.
  43. Bers, D. M. 2001. *Excitation-Contraction Coupling and Cardiac Contractile Force*. Kluwer Academic Publishers, Dordrecht, The Netherlands.
  44. Wilders, R., and H. J. Jongsma. 1993. Beating irregularity of single pacemaker cells isolated from the rabbit sinoatrial node. *Biophys. J.* 65:2601–2613.
  45. Saffitz, J. E., J. G. Laing, and K. A. Yamada. 2000. Connexin expression and turnover: implications for cardiac excitability. *Circ. Res.* 86:723–728.
  46. Boyett, M. R., H. Honjo, and I. Kodama. 2000. The sinoatrial node, a heterogeneous pacemaker structure. *Cardiovasc. Res.* 47:658–687.
  47. Hüser, J., L. A. Blatter, and S. L. Lipsius. 2000. Intracellular  $\text{Ca}^{2+}$  release contributes to automaticity in cat atrial pacemaker cells. *J. Physiol.* 524:415–422.
  48. Bogdanov, K. Y., T. M. Vinogradova, and E. G. Lakatta. 2001. Sinoatrial nodal cell ryanodine receptor and  $\text{Na}^{+}$ - $\text{Ca}^{2+}$  exchanger: molecular partners in pacemaker regulation. *Circ. Res.* 88:1254–1258.
  49. Sutko, J. L., J. A. Airey, W. Welch, and L. Ruest. 1997. The pharmacology of ryanodine and related compounds. *Pharmacol. Rev.* 49:53–98.
  50. Hille, B. 2001. *Ionic Channels of Excitable Membranes*. Sinauer Associates, Sunderland, MA.
  51. Cheng, H., W. J. Lederer, and M. B. Cannell. 1993. Calcium sparks: elementary events underlying excitation-contraction coupling in heart muscle. *Science*. 262:740–744.
  52. Guevara, M. R., and T. J. Lewis. 1995. A minimal single-channel model for the regularity of beating in the sinoatrial node. *Chaos*. 5:174–183.
  53. Lipsius, S. L., J. Hüser, and L. A. Blatter. 2001. Intracellular  $\text{Ca}^{2+}$  release sparks atrial pacemaker activity. *News Physiol. Sci.* 16:101–106.
  54. Durgan, D. J., M. A. Hotze, T. M. Tomlin, O. Egbejimi, C. Graveleau, E. D. Abel, C. A. Shaw, M. S. Bray, P. E. Hardin, and M. E. Young. 2005. The intrinsic circadian clock within the cardiomyocyte. *Am. J. Physiol. Heart Circ. Physiol.* 289:H1530–H1541.

55. Vinogradova, T. M., A. E. Lyashkov, W. Z. Zhu, A. M. Ruknudin, S. Sirenko, D. M. Yang, S. Deo, M. Barlow, S. Johnson, J. L. Caffrey, Y. Y. Zhou, R. P. Xiao, H. P. Cheng, M. D. Stern, V. A. Maltsev, and E. G. Lakatta. 2006. High basal protein kinase A-dependent phosphorylation drives rhythmic internal  $\text{Ca}^{2+}$  store oscillations and spontaneous beating of cardiac pacemaker cells. *Circ. Res.* 98:505–514.
56. Meek, W. J., and J. A. E. Eyster. 1914. Experiments on the origin and propagation of the impulse in the heart IV. The effect of vagal stimulation and of cooling on the location of the pacemaker within the sino-auricular node. *Am. J. Physiol.* 34:368–383.
57. Boineau, J. P., R. B. Schuessler, W. R. Roeske, L. J. Autry, C. B. Miller, and A. C. Wylds. 1983. Quantitative relation between sites of atrial impulse origin and cycle length. *Am. J. Physiol. Heart Circ. Physiol.* 245:H781–H789.
58. Schuessler, R. B., J. P. Boineau, and B. I. Bromberg. 1996. Origin of the sinus impulse. *J. Cardiovasc. Electrophysiol.* 7:263–274.
59. Shibata, N., S. Inada, K. Mitsui, H. Honjo, M. Yamamoto, R. Niwa, M. R. Boyett, and I. Kodama. 2001. Pacemaker shift in the rabbit sinoatrial node in response to vagal nerve stimulation. *Exp. Physiol.* 86:177–184.
60. Roberts, L. A., G. R. Slocum, and D. A. Riley. 1989. Morphological study of the innervation pattern of the rabbit sinoatrial node. *Am. J. Anat.* 185:74–88.
61. Beau, S. L., D. E. Hand, R. B. Schuessler, B. I. Bromberg, B. Kwon, J. P. Boineau, and J. E. Saffitz. 1995. Relative densities of muscarinic cholinergic and beta-adrenergic receptors in the canine sinoatrial node and their relation to sites of pacemaker activity. *Circ. Res.* 77:957–963.
62. Winfree, A. T. 1967. Biological rhythms and the behavior of populations of coupled oscillators. *J. Theor. Biol.* 16:15–42.
63. Jalife, J. 1984. Mutual entrainment and electrical coupling as mechanisms for synchronous firing of rabbit sino-atrial pace-maker cells. *J. Physiol.* 356:221–243.
64. Verheijck, E. E., R. Wilders, R. W. Joyner, D. A. Golod, R. Kumar, H. J. Jongsma, L. N. Bouman, and A. C. van Ginneken. 1998. Pacemaker synchronization of electrically coupled rabbit sinoatrial node cells. *J. Gen. Physiol.* 111:95–112.
65. Michaels, D. C., E. P. Matyas, and J. Jalife. 1987. Mechanisms of sinoatrial pacemaker synchronization: a new hypothesis. *Circ. Res.* 61:704–714.
66. Mark, G. E., and F. F. Strasser. 1966. Pacemaker activity and mitosis in cultures of newborn rat heart ventricle cells. *Exp. Cell Res.* 44:217–233.
67. Harary, I., and B. Farley. 1963. In vitro studies on single beating rat heart cells. I. Growth and organization. *Exp. Cell Res.* 29:451–465.
68. Pumir, A., A. Arutunyan, V. Krinsky, and N. Sarvazyan. 2005. Genesis of ectopic waves: role of coupling, automaticity, and heterogeneity. *Biophys. J.* 89:2332–2349.
69. Rigg, L., and D. A. Terrar. 1996. Possible role of calcium release from the sarcoplasmic reticulum in pacemaking in guinea-pig sino-atrial node. *Exp. Physiol.* 81:877–880.
70. Bers, D. M. 2002. Calcium and cardiac rhythms: physiological and pathophysiological. *Circ. Res.* 90:14–17.
71. Cerbai, E., R. Pino, L. Sartiani, and A. Mugelli. 1999. Influence of postnatal-development on  $I_f$  occurrence and properties in neonatal rat ventricular myocytes. *Cardiovasc. Res.* 42:416–423.
72. Gaughan, J. P., C. A. Hefner, and S. R. Houser. 1998. Electrophysiological properties of neonatal rat ventricular myocytes with  $\alpha$ 1-adrenergic-induced hypertrophy. *Am. J. Physiol. Heart Circ. Physiol.* 275:H577–H590.
73. Er, F., R. Larbig, A. Ludwig, M. Biel, F. Hofmann, D. J. Beuckelmann, and U. C. Hoppe. 2003. Dominant-negative suppression of HCN channels markedly reduces the native pacemaker current  $I_f$  and undermines spontaneous beating of neonatal cardiomyocytes. *Circulation.* 107:485–489.
74. BoSmith, R. E., I. Briggs, and N. C. Sturgess. 1993. Inhibitory actions of ZENECA ZD7288 on whole-cell hyperpolarization activated inward current ( $I_f$ ) in guinea-pig dissociated sinoatrial node cells. *Br. J. Pharmacol.* 110:343–349.
75. Robinson, R. B., and S. A. Siegelbaum. 2003. Hyperpolarization-activated cation currents: from molecules to physiological function. *Annu. Rev. Physiol.* 65:453–480.
76. Bub, G., L. Glass, N. G. Publicover, and A. Shrier. 1998. Bursting calcium rotors in cultured cardiac myocyte monolayers. *Proc. Natl. Acad. Sci. USA.* 95:10283–10287.
77. Hwang, S. M., T. Y. Kim, and K. J. Lee. 2005. Complex-periodic spiral waves in confluent cardiac cell cultures induced by localized inhomogeneities. *Proc. Natl. Acad. Sci. USA.* 102:10363–10368.
78. Rohr, S., and J. P. Kucera. 1997. Involvement of the calcium inward current in cardiac impulse propagation: induction of unidirectional conduction block by nifedipine and reversal by Bay K 8644. *Biophys. J.* 72:754–766.
79. Marvin, W. J. Jr., V. L. Chittick, J. K. Rosenthal, A. Sandra, D. L. Atkins, and K. Hermsmeyer. 1984. The isolated sinoatrial node cell in primary culture from the newborn rat. *Circ. Res.* 55:253–260.
80. Silva, J., and Y. Rudy. 2003. Mechanism of pacemaking in  $I_f(K1)$ -downregulated myocytes. *Circ. Res.* 92:261–263.
81. Bick, R. J., M. B. Snuggs, B. J. Poindexter, L. M. Buja, and W. B. Van Winkle. 1998. Physical, contractile and calcium handling properties of neonatal cardiac myocytes cultured on different matrices. *Cell Adhes. Commun.* 6:301–310.
82. Kilborn, M. J., and D. Fedida. 1990. A study of the developmental changes in outward currents of rat ventricular myocytes. *J. Physiol.* 430:37–60.
83. Guo, W., K. Kamiya, J. Cheng, and J. Toyama. 1996. Changes in action potentials and ion currents in long-term cultured neonatal rat ventricular cells. *Am. J. Physiol. Cell Physiol.* 271:C93–C102.
84. Gaudesius, G., M. Miragoli, S. P. Thomas, and S. Rohr. 2003. Coupling of cardiac electrical activity over extended distances by fibroblasts of cardiac origin. *Circ. Res.* 93:421–428.
85. Miragoli, M., G. Gaudesius, and S. Rohr. 2006. Electrotonic modulation of cardiac impulse conduction by myofibroblasts. *Circ. Res.* 98:801–810.
86. Orita, H., M. Fukasawa, S. Hirooka, H. Uchino, K. Fukui, and M. Washio. 1993. Modulation of cardiac myocyte beating rate and hypertrophy by cardiac fibroblasts isolated from neonatal rat ventricle. *Jpn. Circ. J.* 57:912–920.
87. Peng, C. K., J. Mietus, J. M. Hausdorff, S. Havlin, H. E. Stanley, and A. L. Goldberger. 1993. Long-range anticorrelations and non-Gaussian behavior of the heartbeat. *Phys. Rev. Lett.* 70:1343–1346.
88. Turcott, R. G., and M. C. Teich. 1996. Fractal character of the electrocardiogram: distinguishing heart-failure and normal patients. *Ann. Biomed. Eng.* 24:269–293.
89. Ivanov, P. C., L. A. N. Amaral, A. L. Goldberger, S. Havlin, M. G. Rosenblum, Z. R. Struzik, and H. E. Stanley. 1999. Multifractality in human heartbeat dynamics. *Nature.* 399:461–465.
90. Mäkilä, A. M., T. H. Mäkilä, J. T. Korpeläinen, K. A. Sotaniemi, H. V. Huikuri, and V. V. Myllylä. 2004. Heart rate dynamics predict poststroke mortality. *Neurology.* 62:1822–1826.